TRACER KINETIC ANALYSIS OF POSITRON TOMOGRAPHIC STUDIES

DOPAMINE METABOLISM QUANTIFIED IN THE HUMAN BRAIN: TRACER KINETIC ANALYSIS OF POSITRON TOMOGRAPHIC STUDIES

By

LINDA MARIE WAHL

A Thesis

Submitted to the School of Graduate Studies

in Partial Fulfilment of the Requirements

for the Degree

Master of Science

McMaster University

MASTER OF SCIENCE (1992) McMASTER UNIVERSITY
(Physics) Hamilton, Ontario

TITLE: Dopamine Metabolism Quantified in the Human Brain:
Tracer Kinetic Analysis of Positron Tomographic Studies

AUTHOR: Linda Marie Wahl, B.A.Sc. (University of Waterloo)

SUPERVISOR: Professor C. Nahmias

NUMBER OF PAGES: xii, 135

Abstract

Mathematical models are used to estimate physiological parameters which are otherwise inaccessible to measurement. When applied to tracer kinetic data obtained in positron tomographic studies, these methods allow for the quantitative analysis of regional metabolic rates in the human brain during life.

Dopamine, a neurotransmitter in the mammalian central nervous system, is synthesized by the action of aromatic amino acid decarboxylase on L-dihydroxyphenylalanine (L-dopa). A fluorinated analogue of L-dopa, 6-[^{18}F]fluoro-L-dopa, is used as a tracer in positron tomography to study the nigrostriatal dopaminergic system. Although this tracer has been in use in man for over ten years, a definitive method of quantitative analysis has not yet emerged. The comparison of quantitative results obtained by this approach has been confounded by the diversity of mathematical modelling techniques employed. These techniques range from simple graphical analyses, which yield a single rate constant for the entire system, to complex compartmental approaches, which may not present a unique solution.

The goal of this research has been to develop an approach to quantitative analysis which is both informative and mathematically justifiable. Compartmental models of increasing complexity have been evaluated by statistical methods (F-test) to

determine the simplest model which adequately fits the data. This strict methodological approach indicates that a two-compartment, three-parameter model produces the best fit, in a statistical sense, to the measured data. This data has also been analyzed by a simple graphical method to yield an influx constant for the system. The influx constant has also been calculated, for comparison, from the results of the compartmental analysis.

The two methods were found to be in excellent agreement; both responded predictably to physiological perturbations of the system. While the compartmental method yielded a more informative analysis of the system, the graphically determined influx constant was found to be less sensitive to measurement errors. It is recommended that these two methods be applied in parallel, such that the comparison of results may serve as an internal measure of the integrity of the analysis.

Acknowledgements

The Department of Nuclear Medicine at Chedoke-McMaster Hospitals, and the Department of Physics and Astronomy at McMaster University, have jointly made this project possible. I am grateful for the use of their facilities and for the generous assistance of their staff.

This research has been largely shaped by hours of discussion and debate with Dr. E.S. Garnett and Dr. Claude Nahmias. I am indebted to both for their lucid insights and thorough criticism. Dr. Garnett has been relentless in his opposition to mathematical sophistry, and for this I am grateful. I would also like to thank Dr. A.J. Rainbow, the third member of my committee, whose queries and suggestions have been valuable in clarifying my own thinking.

Rob deKemp and Anita Scheffel have been, as they well know, continual sources of advice, encouragement, and technical expertise. I am also thankful to Margo Thompson for her help in the data collection.

The constraints of time and space will limit the expression of my gratitude to my supervisor, Dr. Nahmias. I can simply voice the quiet refrain of the MIND Lab.: *claudamus*.

Table of Contents

List of Figures

List of Tables

Chapter 1

Tracer Kinetics Measured with Positron Tomography

Introduction

Quantitative methods have become increasingly important in the analysis of metabolic processes studied during life. Mathematical models can provide a concise description of the complex dynamic processes which occur in physiology. Such models may be used to estimate physiological quantities that are inaccessible to direct measurement. Parameters such as the rates of chemical reactions or blood flow, during life, can be investigated in this way.

Positron tomography (PET) is a medical imaging technique which allows the regional measurement of dynamic processes. PET combines the concepts of computerized tomography with the use of specific molecules labelled with positron emitting isotopes. Certain molecules can be synthesized so that one atom is replaced by a radioisotope which decays by positron emission. A ring of radiation detectors are positioned around an object which contains such isotopes. The techniques of computerized tomography are then used to reconstruct the spatial distribution of the labelled molecules in a cross-section of the object.

The Use of Tracers in Positron Tomography

Certain molecules may be labelled with positron emitting isotopes and introduced into the human blood stream. The distribution of radioactivity in the field of view of the tomograph then represents the distribution of the radiolabel in, for example, a cross-section of the head. Mathematical techniques can then be used to estimate such parameters as the rates of chemical reactions which involve the labelled molecule.

Provided that the labelled molecule is introduced in sufficiently small quantities, the overall kinetics of the chemical reactions under study will not be altered; in this case the labelled molecule is called a "tracer". In some cases, it is further assumed that the tracer is transported and metabolized at the same rate as the compound being traced. This assumption is clearly valid when the labelled molecule is chemically identical to the native compound. In such cases, the tracer is biologically indistinguishable from the unlabelled molecule. In the case of "tracer analogues", labelled molecules which are not identical to the compound being traced, appropriate correction factors may have to be applied (Nahmias, 1985, p. 190).

In addition, positron tomography cannot distinguish among the various chemical species that may be labelled, such as the original labelled molecule and any of its metabolites. Strategies may be employed to ensure that radioactivity is contained

exclusively in the injected molecule, or in metabolites specific to the chemical reaction under study. Mathematical techniques may also be used to separate the contributions of the various labelled species to the measured radioactivity.

When these conditions are met, the rates of chemical reactions in specific regions of the living brain may be measured.

Positron Tomography

Certain molecules of biological interest can be synthesized so that one atom is replaced by a proton rich nuclide, which may decay by the emission of a positron, a positively charged electron. As the ejected positron travels through matter, it loses kinetic energy through excitation and ionization events. Once the positron is sufficiently slow, it will pair with an electron in the medium. The two particles will annihilate, usually disposing of their rest energy by the emission of two photons of equal energy in opposite directions (Evans, 1955).

A ring of radiation detectors can be positioned around an object which contains positron emitting isotopes. When two photons are detected simultaneously by different detectors in the ring, it can be assumed that an annihilation event occurred somewhere

along the line joining the two detectors. These annihilation events will occur, within the range of a positron in the medium, at the sites of radioactive decay, and hence very close to the location of a labelled molecule.

When a sufficient number of such "coincidence" events has been accumulated, an algorithm for image reconstruction from projections can be used (Nahmias, 1985, pp. 94-117; Herman, 1980). This technique transforms the values of line integrals of a parameter measured through an object to a distribution of the parameter in a cross-section of the object. In this way the spatial distribution of radioactivity, and therefore of the positron emitting label, can be recovered. When several of these images are acquired sequentially, the time course of radioactivity in, for instance, a certain region of a cross-section of the brain can be constructed.

The spatial resolution of the images created by positron tomography is limited by several factors. The range in tissue of positrons emitted by isotopes of biological interest is typically less than 2 mm (Cho et al., 1975). Emitted photons will deviate by about 0.5 degrees from strict colinearity (Evans, 1955). Finally, the energy of these photons (511 keV) determines the type and size of detector which must be used.

At McMaster University, the tomograph which is currently in use is a Siemens ECAT 953. This tomograph uses sixteen rings of bismuth germanate crystals to reconstruct 31 contiguous cross-sectional planes. Both the axial and transaxial

resolutions of the scanner are about 6 mm (FWHM). The volume scanned is a cylinder, 40 cm in diameter and 10.8 cm in length.

One label that is used in positron tomography is a radioisotope of fluorine, [18F]. This isotope decays by emitting a positron with a maximum energy of 0.633 MeV, a most probable energy of 0.203 MeV, and a range in water of 1.02 mm (FWHM); the half-life for this radioisotope is 109.7 minutes (Cho et al., 1975).

In a typical study, about 100 μCi/kg of [18F]-labelled molecule will be injected intravenously into a subject. To follow the time-course of the distribution of radioactivity, images are acquired sequentially beginning immediately after the injection. Typically, 12 images at 10 seconds per image may be followed by 6 images of 30 seconds per image, which may be followed by 5 minute images for the remainder of a 2.5 hour study. Over 50 million counts are accumulated over the course of a study. The details of the experimental protocol used in this investigation are provided in Chapter 4.

Mathematical Modelling

Mathematical models can provide a simple, economical description of some of the complex biochemical processes which occur in living organisms. Given a set of

experimental input and output values, a series of equations which relates the outputs to the inputs may be proposed. This series of equations, or *model*, can then be analyzed in a variety of ways, with the goal of gaining deeper understanding of the biological process (Carson et al., 1983).

In the simplest case, the model may serve only to mimic, empirically, the output data. For example, output measurements may be fit to a smooth curve, without attention to the numerical parameters of the curve. In this situation, an understanding of the underlying biological mechanism is not required.

A model may also be proposed which is not only able to mimic the outputs, but to predict the response of the system to different experimental conditions. In this case, the model is able to simulate the biological process to some degree. The predictive value of such a model may facilitate a qualitative understanding of the biological mechanism.

For a quantitative analysis of the underlying biological process, a mathematical model may provide numerical estimates of the parameters of the system. In this case, values such as the rates of chemical reactions may be calculated through the use of the model. Such a model may allow system quantities which are not accessible to measurement to be estimated from the observations of accessible variables.

Compartmental Analysis

A kinetic model is a quantitative model of a system for which the change in system variables over time is of interest. Given a set of input variables, F(t), and a set of output variables, G(t), the general equation of a kinetic model is:

$$G(t) = \int_{\tau=0}^{t} F(\tau)\, H(F, G, t, \tau)\, d\tau \qquad (1)$$

where H(F,G,t,τ) is the *characteristic function* of the system. In this case, the characteristic function is very general, and may depend on both the input and the output variables. Now suppose that this system acts on a substance P, which is metabolized to substance Q. In the general case, the characteristic function may depend upon the amounts of P and Q in the system. If the precursor molecule can be labelled, such that F(P,t) gives the concentration of labelled P at any time t, then the concentration of labelled Q can be given as G(Q,t), such that:

$$G(Q, t) = \int_{\tau=0}^{t} F(P, t)\, H(P, Q, t, \tau)\, d\tau \qquad (2)$$

If the characteristic function does not depend on the output, G(Q,t), the system is said to be *linear*. This implies that the principle of superposition holds, that is, the output for a sum of inputs is equal to the summed output of the individual inputs. If the characteristic is time invariant over the time interval of the experiment, the system

is said to be 'stationary'. In this case, the integral above can be re-written as the convolution (where '*' denotes the operation of convolution):

$$G(Q,t) = \int_{\tau=0}^{t} F(P,t)\,H(P,Q,t-\tau)\,d\tau \qquad (3)$$
$$G(Q,t) = F(P,t) * H(P,Q,t)$$

To perform compartmental analysis, it is assumed that this system is composed of compartments, into which and from which material flows. A *compartment*, for this purpose, is defined as a volume in which the concentration of the material is homogenous. Material may flow between any two compartments and between a compartment and the outside, or external phase. There is at least one input to the system of compartments from the external phase; this corresponds to the input F(P,t) in the general kinetic model. The general mass transfer equation is employed which states that the rate of change of the amount of material in a given compartment is equal to the influx to the compartment minus the efflux from the compartment. This implies that material is neither created nor destroyed within the compartment.

It is further assumed that the rate of efflux from a compartment is dependent only upon the amount of material in the compartment and a rate constant. The flux to compartment i from compartment j can then be written as:

$$p_{ij} = k_{ij} q_j(t) \qquad (4)$$

where $q_j(t)$ is equal to the quantity of material in compartment j at time t. Note that k_{ij} is the fractional rate constant for the transfer of material to compartment i from compartment j, in dimensions of inverse time. In this way, the rate of change of the amount of material in a given compartment can be written as:

$$\frac{dq_i(t)}{dt} = -\sum_{j=0}^{n} k_{ji} q_i(t) + \sum_{j=1}^{n} k_{ij} q_j(t) + \rho_{i0} \qquad (5)$$

for a system of n compartments. Note that the constant k_{0i} is equal to the rate of efflux from compartment i to the external phase, while ρ_{i0} is equal to the influx to compartment i from the external phase.

If the rate constants are time invariant (stationarity condition) and independent of the q_i's (linearity condition), these equations form a set of linear first-order differential equations. From a knowledge of the rate constants, the initial conditions, and the inputs to the system, these equations can be integrated, analytically or numerically, to predict the amount of material in each compartment at any given time. This predicted response of the model, which we will denote y(t), corresponds to G(Q,t) in the general model.

Numerical Solution for the Rate Constants

Consider a compartmental model with n compartments, where $F_i(t)$ represents the amount of precursor input to compartment i at time t. Suppose that the response of the model depends on a set of p rate constants, p_j. Measurements of the output of the model, $z(t_k)$, are taken at m times, t_k. Often, initial conditions are set such that:

$$q_i(0) = 1$$
$$q_j(0) = 0; j = 1, \ldots, n; j \neq i \qquad (6)$$

In this case, the result of the integration corresponds to the response of the system to a spike input to compartment i at time zero. This is the *impulse response* of the model, which is one way of expressing the characteristic of the system, H(P,Q,t). Often, an investigator is unable to measure the response of individual compartments in the model, and is interested in the response of the system as a whole. In this case, the impulse response of the model is the sum of the responses of each of the n compartments to a spike input to compartment i:

$$I(t) = \sum_{j=1}^{n} q_j(t) \qquad (7)$$

In practice, the input function for the system is rarely a perfect spike. Suppose that the precursor is administered to a biological system through the circulation, and

so the input function, denoted $C_p(t)$, represents the amount of labelled precursor in the arterial plasma at any time t. In this case, the convolution of the input function with the impulse response of the model will yield a predicted output for the system:

$$y(t) = C_p(t) * I(t) \qquad (8)$$

Since the input function depends on the values of the rate constants (Equations 5 and 7), the predicted response of the system also depends on these values. The rate constants of the model can therefore be varied until this predicted output most closely matches, in a least squares sense, the measured output of the system. Suppose that the impulse response of the model depends on a set of rate constants, **p**. The weighted least squares estimator then generates an estimate, $\mathbf{p}_m$, that minimizes the weighted sum of squared differences between the observed values, $z(t_k)$, at time t_k, and the model predictions, $y(t_k,\mathbf{p})$. This is referred to as minimizing the weighted residual sum of squares, $r(\mathbf{p})$, or as optimizing the parameters. For a particular set of weights, w_k, this is the minimum of the function:

$$r(\boldsymbol{p}) = \sum_{k=1}^{m} w_k [z(t_k) - y(t_k, \boldsymbol{p})]^2 \qquad (9)$$

When $w_k = 1$ for all k, this is the method of unweighted least squares. However, the choice of weights is best based on some knowledge of the precision of the measured values.

The Choice of Weights

Given p rate constants in the model, the p-by-p covariance matrix of **p**, COV(**p**), gives a measure of the dispersion of **p** about its mean. This reflects the *precision* of **p** as an estimator. The *j*th diagonal entry of COV(**p**) gives the variance of p_j. COV(**p**) can be constructed in the following way:

Recall that $y(t_k,\mathbf{p})$ is the output of the system as predicted by the model. Sensitivity functions are the derivatives of $y(t_k,\mathbf{p})$ with respect to the rate constants. These can be evaluated by a numerical procedure. Let $\mathbf{s}(t,\mathbf{p})$ be an p-dimensional column vector whose *j*th component is $\partial y/\partial p_j$. If **W** is the diagonal matrix of the weights, w_k, then the information matrix for the system is equal to $\mathbf{S}^t.\mathbf{W}.\mathbf{S}$, denoted **M**. An estimate of the covariance matrix can then be obtained by evaluating $v\mathbf{M}^{-1}$. Here v is equal to $r(\mathbf{p}_m)/(m-p)$, that is, the minimum value of the residual divided by the degrees of freedom of the system (Landaw and DiStephano, 1984; Delforge et al., 1991). To summarize:

$$COV(\mathbf{p}) = \frac{r(\mathbf{p}_m)}{m-p}\,[S^t \cdot W \cdot S]^{-1} \qquad (10)$$

It can be shown that the diagonal terms of COV(**p**) are minimized by using weights, w_i, that are inversely proportional to the variance of the error, where the error is the difference at each time point between the measured and predicted outputs (Landaw and DiStephano, 1984). Since radioactive decay can be modelled by Poisson counting statistics, where the variance is proportional to the mean (Enge, 1966), the reciprocal of the measured outputs themselves can be used as weights in the optimization.

The Determination of Model Order

Various statistical methods have been proposed for determining the "best" model to fit the data. While Fourier analysis can be used to establish the number of compartments needed to fit a given data set (the model order), these methods usually require several hundred observations in time, with less than two or three percent noise per observation (Provencher, 1986; Hayden et al., 1983). For PET studies, which typically contain less than 50 time observations and about five percent noise, these methods cannot be used. Instead, the weighted residual sum of squares is evaluated for progressively more complex models, and the "best" model is chosen by means of an F-test. The F statistic is computed as:

$$F=\frac{(r_1-r_2)/(P_2-P_1)}{r_2/(m-P_2)} \sim F(P_2-P_1, m-P_2) \qquad (11)$$

Critical Discussion

Before compartmental analysis can be meaningfully employed, a number of factors must be considered. The assumptions outlined in the derivation, above, must be valid for the system under study. In particular, the conditions of linearity and stationarity must be satisfied. It is generally accepted that a decay curve can be fit to the sum of no more than three decaying exponential functions; this implies that a maximum of three compartments can be resolved with a single data set (Zierler, 1981). If the data are noisy (as is the case with PET), three compartments may still be unresolvable. The optimization procedure may be unable to reach a unique solution in this case. It is critical that only the simplest model which adequately fits the data be used.

When each of the above conditions is met, compartmental analysis is mathematically valid, but it may still be physically meaningless. Unless the physical meanings of the compartments and rate constants can be independently verified, through knowledge of the physical system, independent measures or perturbation studies, the technique is reduced to a curve fitting exercise. While computerized optimization procedures will nearly always produce numerical results, caution must be exercised in experimental design and validation to ensure that this result is meaningful.

Graphical Analysis

Because of the considerations above, it is sometimes valuable to determine one or two "lumped" parameters of the system under study, rather than attempting to solve a compartmental model completely. Graphical analyses involve the construction of a plot of two transformed variables, calculated from the measured variables of the system. The numerical parameters of the system can then be estimated through a regression analysis of this graph. If the plotted points approximate a straight line, for example, the slope and intercept of the line can be estimated. In this way, a graphical method may be used to estimate two parameters of the system.

Consider the example of a two-compartment model pictured in Figure 1.

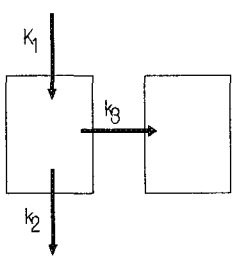

Figure 1: A simple two-compartment, three-parameter model. K_1, k_2, and k_3 are rate-constants in dimensions of inverse time.

Suppose that A(t) is the amount of tracer in the input function at time t, which feeds the left hand compartment through the arrow denoted K_1 in the figure. B(t) and C(t)

are the amounts in the left and right compartments respectively. The flux between the two compartments is given as the amount in the left compartment times the rate constant for this transfer, k_3, which is in units of inverse time. Although K_1 is also in units of inverse time, it is denoted by a capital letter and its units are commonly denoted as, for example, [ml/min/ml]. These notational differences serve to emphasize the fact that, in common physiological situations, this constant contains contributions from two effects: the fraction of available material in the input (often a solute in an input solution) that is transfered per unit time (min^{-1}), and the volume of the input solution that is available per volume of tissue under study (ml/ml).

The differential equations describing this system, by the application of Equation 5, are then:

$$\begin{aligned} \frac{dB}{dt} &= K_1 A - (k_2 + k_3) B \\ \frac{dC}{dt} &= k_3 B \end{aligned} \qquad \textbf{(12)}$$

Integration (assuming initial amounts everywhere are zero) yields:

$$\begin{aligned} B(t) &= K_1 \int_{\tau=0}^{t} A(\tau)\, d\tau - (k_2 + k_3) \int_{\tau=0}^{t} B(\tau)\, d\tau \\ C(t) &= k_3 \int_{\tau=0}^{t} B(\tau)\, d\tau \end{aligned} \qquad \textbf{(13)}$$

and now the second equation can be substituted into the first:

$$B(t) = K_1 \int_{\tau=0}^{t} A(\tau)\, d\tau - \frac{(k_2+k_3)}{k_3} C(t) \qquad \textbf{(14)}$$

This equation can be re-arranged to yield:

$$\frac{B(t)+C(t)}{A(t)} = \frac{K_1 k_3}{(k_2+k_3)} \frac{\int_{\tau=0}^{t} A(\tau)\, d\tau}{A(t)} + \frac{k_2}{(k_2+k_3)} \frac{B(t)}{A(t)} \qquad \textbf{(15)}$$

Now suppose that this system is in equilibrium, that is, there is no net change in the amount of tracer in the first compartment, B(t). (This also implies that there is no change in the amount of tracer in the input function at any time.) In this case, dB/dt will be equal to zero, and:

$$\frac{B(t)}{A(t)} = \frac{K_1}{(k_2+k_3)} \qquad \textbf{(16)}$$

Substituting, we find:

$$\frac{B(t)+C(t)}{A(t)} = \frac{K_1 k_3}{(k_2+k_3)} \frac{\int_{\tau=0}^{t} A(\tau)\, d\tau}{A(t)} + \frac{K_1 k_2}{(k_2+k_3)^2} \qquad \textbf{(17)}$$

Suppose a graph is constructed of the total amount of material in the system at time T versus the integrated amount in the input function up to that time, both normalized by the amount of tracer in the input at t. This equation indicates that, when the system has reached equilibrium, this plot will yield a straight line whose slope and intercept are determined by the rate constants of the model. Note that this graph can be constructed without knowledge of the rate constants, and linear regression may be used to estimate the slope and intercept of the plot. This will yield estimates for the "lumped" slope and intercept parameters.

This type of analysis has been rigorously derived and extended for models with any number of compartments, and has been proven to be valid for situations when the input function is not constant (Patlak et al., 1983; Patlak and Blasberg, 1985). Models which can be solved by this technique include those which contain an *irreversible* compartment, that is, a compartment which has no efflux, a sink. In this case, graphical analysis can be used to determine the *influx constant* of the system, which is a measure of the flow of material through the system and into the irreversible compartment at steady state.

To extend the simple system outlined above, consider a more general compartmental model which has a single source of the solute of interest. The amount of solute in this feed is denoted $C_p(t)$, and may vary with time (this corresponds to A(t)

in the discussion above). Rapid exchange of the solute between the source solution and a set of *reversible* compartments may occur; these compartments are reversible in the sense that they may have influx and efflux between themselves and the source solution. The solute may also enter an irreversible region, from either the source solution or any of the reversible compartments.

Assuming that the solute and any metabolites remain trapped in the irreversible region, that the test solute does not alter the system kinetics, and that the flux between compartments is a first order process, the influx constant of the system can be determined graphically. The influx constant is defined as the steady state rate of flux into the irreversible region, divided by the concentration of the solute in the source solution, *for a constant source concentration.* Steady state occurs when the amount of solute in each of the reversible compartments is constant.

In the analysis of positron tomographic studies, the concentration of the solute is represented by the amount of radioactivity present in a given region. To calculate the influx constant, a graph of normalized activity versus normalized time is plotted. Normalized time is defined to be equal to:

$$x = \frac{\int_{\tau=0}^{t} C_p(\tau)\, d\tau}{C_p(t)} \qquad (18)$$

where $C_p(t)$ is equal to the amount of tracer in the input, or feed, to the system, at time t. Similarly, normalized activity is defined as:

$$y = \frac{A_m(t)}{C_p(t)} \qquad (19)$$

where $A_m(t)$ is equal to the total amount of activity measured in the system.

Intuitively, this normalized time gives the amount of time that a constant input function, at the current value of C_p, would have fed the system to give the same total integrated feed. Normalized activity is the ratio of the amount in the whole system at this point to this constant value. One can imagine that in this transformed or *normalized* system, this ratio will increase quickly while the reversible compartments come into equilibrium, and then increase at a constant rate which reflects the net flux of the solute across the system and into the irreversible compartment. The y-intercept of a fit to the linear portion of this curve would then be a measure of amount of material in the reversible compartments, had they been in equilibrium with the input function at time zero.

In agreement with these intuitive deductions, when normalized activity and normalized time are plotted against each other (a "Patlak plot"), an initial non-linear portion of the curve is followed by a region which can be fitted to a straight line by

regression analysis. The slope of this line is equal to the influx constant of the system, denoted K_i. The intercept has been proven to be less than or equal to the sum of the steady state space of the exchangeable region (the *distribution volume*) and the plasma volume (Patlak et al., 1983). As shown in the preceding example, these constants may also be calculated from a knowledge of the rate constants of the compartmental model. To differentiate between the two methods of estimating K_i, the notation $K_{i,g}$ will refer to the influx constant determined graphically, while $K_{i,c}$ will denote the influx constant as calculated from the compartmental rate constants.

Graphical Analysis for Reversible Systems

Consider the same two-compartment model discussed above, and suppose that k_3 is equal to zero. The model now reduces to that shown in Figure 2. In this case, there will be no further uptake of the tracer after steady state has been reached; the

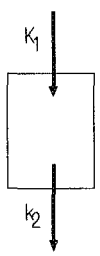

Figure 2: A single compartment, two-parameter model. K_1 and k_2 are rate constants in units of inverse time.

slope of a Patlak plot for this system will be zero. This can be verified by substituting $k_3 = 0$ into the expression for the influx constant.

The differential equation describing this system (see Equation 5) is then:

$$\frac{dB(t)}{dt} = K_1 A(t) - k_2 B(t) \qquad (20)$$

Which, after integration gives:

$$B(t) = K_1 \int_{\tau=0}^{t} A(\tau)\, d\tau - k_2 \int_{\tau=0}^{t} B(\tau)\, d\tau \qquad (21)$$

After dividing by k_2, and re-arranging, we find:

$$\frac{\int_{\tau=0}^{t} B(\tau)\, d\tau}{B(t)} = \frac{K_1}{k_2} \frac{\int_{\tau=0}^{t} A(\tau)\, d\tau}{B(t)} - \frac{1}{k_2} \qquad (22)$$

Suppose that a graph is constructed of the integrated amount of material in the compartment up to time T, versus the integrated amount in the input function, both

normalized to the amount in the compartment at that time. Then equation 22 indicates that this graph will be linear, with a slope equal to the distribution volume of the tracer in the compartment (K_1/k_2) and an intercept which is equal to the negative reciprocal of k_2.

Note that both axes of this graph are in units of time. Intuitively, the x-axis gives the amount of time it would take for a constant input at a given concentration (B(t)) to reach the integrated input amount which has been reached at the current time. The y-axis gives the amount of time it would take to reach the current integrated amount in the compartment, if the amount in the compartment had been constant and equal to B(t) since time zero. The ratio of these two times will then give the ratio of the amounts of the tracer in the input function and the compartment.

This technique has been formally derived and expanded by Logan et al. (1990), to include any number of reversible compartments in the system. Using the notation of Patlak, a "Logan plot" is a graph of the time integral of $A_m(\tau)$ up to time t versus the time integral of $C_p(\tau)$ up to that time, both normalized by $A_m(t)$. It has been shown that the slope of this plot is equal to the sum of the steady state space of the tracer and the plasma volume (Logan et al., 1990). This slope, as demonstrated in the preceding example, can also be calculated from the rate constants of the model. Note that a Patlak plot of a region with no irreversible trapping will yield zero slope and an intercept which is less than or equal to the slope of a Logan plot for this data.

Critical Discussion

These methods of graphical analysis enable the evaluation of lumped parameters in situations (common in PET) where the concentration of the solute in the source solution cannot be held constant without enormous difficulty. The analyses are relatively model independent: the Patlak model only assumes that the system has a single source and an irreversible region; the Logan plot assumes a single source and no irreversible region. The slope or linearity of the curves produced by these methods serves as an indicator of the validity of the assumptions. While the precise physical interpretation of the compartments may be unknown, the influx constant is a model-independent measure of the storage or *trapping* of the solute in the system, while the distribution volume measures the amount of material which has come into equilibrium with the input function, relative to the input concentration.

Unfortunately, further information about the individual rate constants of the system are not available in this type of analysis. Care must be exercised in defining the *linear* portion of the curve (to which the regression is applied), and in collecting data over a sufficiently long time interval. Finally, the conditions of stationarity and linearity must be verified as in compartmental analysis.

Conclusion

It is clear, then, that both compartmental and graphical methods may be used in the analysis of tracer kinetic data obtained by positron tomography. These methods allow for a quantitative evaluation of the time-course of radioactivity in the brain after the injection of a radio-labelled tracer. In order to interpret meaningfully the results of these analyses, however, knowledge of the transport and metabolism of the tracer must be applied.

Chapter 2

F-dopa as a tracer for Human Dopaminergic Function

Introduction

Information is transmitted within the brain by the nerve cells, called neurons. A neuron is composed of a main body, the soma, a single axon which conducts away from the soma, and many thin projections which conduct towards the soma, called dendrites. Along a neuron, information is transmitted in the form of electricity, the action potential, which is a change in the membrane potential of the body or axon of the neuron. Neurons interact with each other at junctions called synapses; the information is transmitted across these junctions through specific chemicals called neurotransmitters. A neurotransmitter is a molecule which is synthesized and released by the pre-synaptic neuron, and recognized by the post-synaptic neuron. These molecules bind to specific receptors on the surface of the post-synaptic neuron, producing an excitatory or inhibitory effect (Axelrod, 1974).

Over forty possible neurotransmitters have been identified (Iversen, 1982). The catecholamines are a class of neurotransmitters that comprises dopamine, norepinephrine and epinephrine. Dopamine usually has an inhibitory effect. It is mostly found in

nigrostriatal neurons, nerves that originate in a nuclear mass in the mid-brain called the substantia nigra, and end in the corpus striatum, part of the large subcortical mass termed the basal ganglia. The striatum is composed of the caudate nucleus and the putamen. The nigrostriatal information pathways influence various voluntary motor activities (Burnham, 1989).

Disturbances in dopamine metabolism are a key feature in neuro-degenerative disorders such as Parkinson's disease (Agid, 1991). Because of this clinical interest, and because dopaminergic areas are well-localized within the brain, this neurotransmitter is an ideal focus for investigation by positron tomography.

The Synthesis and Metabolism of Dopamine

Dopamine is formed within neurons by the action of L-aromatic amino acid decarboxylase (AADC) on its immediate precursor, 3,4-dihydroxyphenylalanine (L-dopa). L-Dopa is formed from tyrosine by the action of tyrosine hydroxylase; this is the rate limiting step in dopamine synthesis in the brain. Because AADC is normally present in excess in neurons, only insignificant quantities of L-dopa itself are found in the brain. Quantities of L-dopa normally found in the cerebrospinal fluid and the blood are also insignificant.

Dopamine is stored in intraneuronal vesicles, from which it is released when

the nerve cell fires. These vesicles protect the transmitter from catabolic inactivation, by intracellular monoamine oxidase (MAO) or catechol-O-methyl transferase (COMT). The latter enzyme is primarily located on the outer plasma membrane of nearly all cells, and can thus act on neuronal and extraneuronal catecholamines. The major metabolites of dopamine, through the action of MAO and COMT respectively, are dihydroxyphenyl acetic acid (DOPAC) and homovanillic acid (HVA). DOPAC itself also acts as a substrate for COMT, producing homovanillic acid.

The diffusion of molecules from the capillaries to tissue is more restricted in the brain than in other organs of the body. This "blood-brain barrier" is thought to be due, in part, to the tight packing of the endothelial cells which line the capillaries in the brain (Bradbury, 1979, pp. 82-83); some enzymatic mechanisms within this capillary wall may also have an influence (Bertler et al., 1966).

Although dopamine in the circulation does not cross the blood-brain barrier, L-dopa, the immediate precursor for dopamine, is able to enter the brain (Bradbury, 1979, pp. 325-329). L-dopa can thus be labelled with a positron emitting isotope and administered intravenously, in order to study dopaminergic metabolism in the brain by positron tomography. L-dopa, however, also acts as a substrate for COMT, forming O-methyldopa (OMD). OMD, formed in peripheral organs or the circulation, is able to cross the blood-brain barrier. Similarly, OMD formed from L-dopa in the brain is able to enter the blood from the brain.

In the past twenty-five years, the synthesis and metabolism of dopamine in the striatum have been studied by many investigators, employing a variety of methods. These studies have contributed to the understanding of the blood-brain barrier, the synthesis of dopamine from endogenous tyrosine, and dopamine synthesis from exogenously administered dopa. Various positron tomographic studies have also been completed.

A Review of the Literature

The Clinical Impetus

Hornykiewicz (1963) first described low dopamine concentrations in association with Parkinson's disease, a movement disorder characterized by akinesia, rigidity and tremor. Since L-dopa is a known precursor of dopamine, and since L-dopa is able to cross the blood-brain barrier, it was hoped that low dopamine concentrations could be alleviated by the administration of exogenous L-dopa. Various studies of the therapeutic effects of L-dopa administration in Parkinsonian patients were thus undertaken (for example, McGeer and Zeldowicz., 1964), but the efficacy of this treatment remained in debate until the studies of Cotzias et al. (1967). Cotzias found that much higher doses than previously imagined were needed to effect an improvement in some patients. While this result was promising, various side-effects, such as a deficiency of white blood cells, were also reported (Cotzias et al., 1967).

In an attempt to reduce these side effects, which were associated with high dopamine concentrations in the circulation, Papavasiliou et al. investigated the use of a peripheral decarboxylase inhibitor given with therapeutic doses of L-dopa. Less L-dopa was needed for symptomatic control when it was given along with alpha-methyldopa hydrazine, which blocks the conversion of L-dopa to dopamine in peripheral tissues (Papavasiliou, 1972). The clinical effectiveness of various dopa decarboxylase inhibitors, administered with L-dopa, has been compared by Lieberman et al. (1978).

In parallel with these clinical trials, research into the pathology of Parkinson's disease continued. Lloyd and Hornykiewicz reported a decrease in dopa decarboxylase activity in the Parkinsonian brain (Lloyd and Hornykiewicz, 1970). This result was investigated further by Nagatsu et al., who found that tyrosine hydroxylase activity was decreased in the striatum of twelve patients with Parkinson's disease, while dopa decarboxylase activity was decreased in only eight of the twelve patients studied (Nagatsu et al., 1981).

These studies and others have provided the impetus for continued investigations of the synthesis and metabolism of striatal dopamine, in both healthy individuals and patients with Parkinson's disease.

The Synthesis and Metabolism of Dopamine in the Striatum

In 1962, Lovenberg et al. used enzyme preparations from guinea pig kidney and specific inhibitors to establish the presence of a single enzyme in mammalian tissue which catalyzes the decarboxylation of such amino acids as phenylalanine, L-3,4-dihydroxyphenylalanine (L-dopa) and L-tyrosine. It was suggested that this enzyme be referred to as Aromatic L-Amino Acid Decarboxylase (AADC). Evidence was also presented that this enzyme is present in other mammalian tissues, including the brain (Lovenberg et al., 1962).

Two years later, Nagatsu et al. demonstrated the existence of a specific hydroxylase that catalyzes the conversion of L-tyrosine to dopa. This enzyme was referred to as tyrosine hydroxylase, and was found within the brain, adrenal medulla, and sympathetically innervated tissues (Nagatsu et al., 1964).

Bertler et al. used a combination of chemical and histochemical methods to demonstrate that L-dopa, but not D-dopa or dopamine, readily penetrates through the luminal surface of the capillary endothelial cells of the mammalian central nervous system. Both AADC and monoamine oxidase (MAO) were found to be present within the pericytes and endothelial cells of these capillaries. It was inferred that these enzymes in the cells of the capillary wall form an enzymatic barrier for L-dopa. No specific storage mechanism was found for the dopamine formed within the capillary

walls, although it was found in both the nuclear region and cytoplasm of the pericytes and endothelial cells. Dopamine was found to disappear rapidly from these regions unless the action of MAO was inhibited (Bertler et al., 1966).

In summary, these studies have shown that dopamine is formed in the brain through the action of AADC on L-dopa. L-dopa may be formed endogenously by the hydroxylation of native tyrosine, and L-dopa in the blood is able to enter the endothelial cells of capillaries in the brain.

The Blood-Brain Barrier --

Using a carotid injection technique, the uptake of L-dopa, relative to a diffusion marker (tritiated water), was examined by Wade and Katzman. Results indicated that no significant regional differences in L-dopa penetration or AADC activity exist in the capillaries of the rat brain. By examining the uptake of L-dopa at various injectant concentrations, it was concluded that the movement of L-dopa into the brain is a combination of a saturable, mediated-transport system and a non-saturable, diffusion-like mechanism. It was found that this diffusion-like process played only a minor role, accounting for less than 5% of total transport, until concentrations of L-dopa in the injectant exceeded 0.2 mM (injectant concentrations for PET studies which use F-dopa are typically in the μM range). At low concentrations, approximately 70% of L-dopa entering the brain was decarboxylated within 15 seconds. Fluorescence techniques

revealed the presence of L-dopa or dopamine diffusely in the endothelial cytoplasm, with accumulations in the nuclear regions of endothelial cells and the surrounding pericytes. This fluorescence was evident at 15 seconds, peaked at 30 seconds, and had nearly disappeared by 75 seconds after the injection (Wade and Katzman, 1975).

The contribution of the microvessels to the blood-brain barrier was examined by Hjelle et al., who compared the uptake of another diffusion marker, sucrose, to the uptake of three large neutral amino acids (leucine, tyrosine and valine). It was concluded that a selective carrier system was involved in the transport of these amino acids across the blood-brain barrier; stereo-specificity and cross-competition were also exhibited by the amino acids studied. Since uptake of these compounds was found to be similar on both sides of the microvascular wall (as investigated *in situ* and in suspension), it was suggested that this transport mechanism is "not asymmetric" (Hjelle et al., 1978).

In 1990, Knudsen et al. studied the transport of four large neutral amino acids (leucine, phenylalanine, tryptophan and tyrosine) across the blood-brain barrier. Thirty patients who were hospitalized for various disorders requiring carotid angiograms were studied prior to the diagnostic procedure. A bolus of ^{14}C- and ^{3}H-labeled tracer was injected into the internal carotid artery, while radioactivity was measured in blood samples obtained from a second catheter in one of the internal jugular veins. Both single and double membrane models of the blood-brain barrier were analyzed. In

contrast to the results of Hjelle, it was concluded that the transport of amino acids across the blood-brain barrier in humans is asymmetrical, with forward and reverse rate constants differing by an order of magnitude (Knudsen et al., 1990).

The movement of L-dopa from the blood to the brain is then accomplished primarily by a saturable, mediated-transport system. This system is stereo-specific, and the presence of other large neutral amino acids produces a competitive effect. Recent work indicates that the reverse transport process, from the brain to the blood, may not be symmetrical with this process.

Synthesis of Dopamine through Tyrosine Hydroxylase --

Korf et al. examined the effects of electrical stimulation of the nigrostriatal pathway on the metabolism of dopamine in the rat. While stimulation increased the concentration of HVA in the rat brain, dopamine concentrations remained constant. Korf et al. used this result, in combination with the results of other researchers, to conclude that newly synthesized dopamine, from tyrosine, is preferentially released and metabolized. The existence of two storage compartments for striatal dopamine was postulated: a rapidly releasable pool, where dopamine synthesis was regulated; and a second pool which may only be indirectly involved with dopaminergic neurotransmission (Korf et al., 1976).

Labelled tyrosine and the measurement of tritiated water were used to investigate dopamine synthesis *in vitro* and *in vivo*. The rate of tyrosine hydroxylation can be estimated *in vivo* by measuring the quantities of tritiated water formed during the conversion of tritium-labeled tyrosine into [^{3}H]dopa. A decreased rate of tyrosine hydroxylation, contributing to a reduced rate of dopamine synthesis, was observed to follow increases in synaptic dopamine concentrations (Westfall et al., 1976). This result provides direct support for the concept of an inhibitory effect of released dopamine on dopamine synthesis, through the activation of autoreceptors on dopaminergic nerve terminals.

The same method was used to observe changes in the nigrostriatal dopaminergic system after partial destruction by the injection of 6-hydroxydopamine to the substantia nigra (Agid et al., 1973). Increases in tyrosine hydroxylase activity were observed in dopaminergic neurons which survived the lesion.

The acceleration of dopamine synthesis induced by an acute injection of neuroleptics was also demonstrated by this method (Javoy et al., 1974). This effect is mainly related to an increased firing rate in pre-synaptic neurons, resulting from the blockade of post-synaptic receptor sites. An overview of these studies, and related work, is provided by Glowinski (Glowinski, 1976).

These results suggest the existence of two storage compartments for striatal

dopamine, with newly synthesized dopamine (from tyrosine) being preferentially released. Released dopamine has an inhibitory effect on tyrosine hydroxylase activity, while the activity of this enzyme is increased in neurons which survive a partial lesion. Neuroleptics increase the firing rate of dopaminergic neurons.

Dopamine Synthesis from Exogenous L-dopa --

Hefti et al. produced unilateral nigrostriatal lesions in rats by the injection of 6-hydroxydopamine. Comparisons between the lesioned and normal sides were used to establish the site of dopamine formation in the striatum after the administration of exogenous L-dopa. AADC activity was observed "predominantly, but not exclusively" within afferent dopaminergic neurons; these neurons accounted for about eighty percent of the dopamine formed from exogenous dopa. Eight percent of dopamine formation was attributed to the action of AADC in interneurons or in efferent neurons; this dopamine was found to be functionally effective, that is, it appeared to affect the post-synaptic neurons. Six percent of the dopamine was formed in non-neuronal tissue, for example, in the capillary endothelium. An increased firing rate, associated with an increase in transmitter synthesis, was again reported in neurons which survive a nigrostriatal lesion. This increase, however, was not associated with an increased ability to form dopamine from exogenous L-dopa. It was concluded that an acceleration of dopamine synthesis from endogenous tyrosine does not affect dopamine formation from exogenous L-dopa (Hefti et al., 1981).

Evidence that labelled dopamine is stored in neuronal vesicles has been presented by Diffley et al., who use a ^{19}F nuclear magnetic resonance technique in the direct observation of 6-fluorodopamine in guinea pig nerve microsacs. It was demonstrated through this method that 6-fluorodopamine is associated with the vesicles of striatal nerve terminals (Diffley et al., 1983).

Horne et al. conducted an autoradiographic and biochemical study of the cerebral metabolism of exogenous ^{14}C- and ^{3}H-labeled L-dopa. Radioactivity was observed to accumulate in the vesicles of nigrostriatal dopaminergic neurons. The radiolabel was "primarily present in the dopamine molecule during the period of maximal selective accumulation in the striatum". Five minutes after the injection, the distribution of radioactivity was correlated to blood flow measurements. At forty-five minutes, two hours and four hours after injection, accumulation was correlated to endogenous catecholamine content. It was further reported that 3-O-methyldopa accumulated in striatal and cerebellar tissue at approximately the same rate as in the plasma (Horne et al., 1984).

In summary, dopamine is formed after the administration of L-dopa primarily by the action of AADC in dopaminergic neurons. In the case of three labelled analogues of L-dopa, the dopamine so formed appears to be retained in the vesicles of these neurons. Changes in the rate of endogenous dopamine synthesis may not affect dopamine synthesis from exogenous L-dopa.

Recent Work --

The metabolism of F-dopa in the rat was studied by Reith et al., using "donor" rats to synthesize various concentrations of OMFD (1990). Blood samples from these rats, taken at various times and thus containing various proportions of F-dopa and OMFD, were injected into recipient rats. The differential equations describing the time course of OMFD and F-dopa in the blood and brain were integrated and re-arranged so that graphical techniques could be used to estimate the parameters of the system. In this way, the permeability of the blood-brain barrier to OMFD and F-dopa, the fractional clearance from the brain of F-dopa, and the F-dopa decarboxylation rate constant were determined. The latter value was found to be less than one percent of the rate of striatal decarboxylation of L-dopa reported in the literature. This finding was interpreted as further evidence that the striatum has two dopamine pools, of which only dopamine in the larger pool is protected from metabolism. It was suggested that the large amounts of fluorodopamine which were synthesized during the experiment could not be accommodated by the striatal vesicles, and thus ninety-nine percent of the newly synthesized fluorodopamine was released and metabolized, while only one percent was trapped in the large DA pool (Reith, 1990).

The metabolism of F-dopa and [^{3}H]L-dopa was also compared by Melega et al. in live rats. In agreement with our earlier studies (see Garnett et al., 1987, below),

F-dopa was found to clear from the blood more rapidly than native dopa. It was postulated that this difference may be due to rapid methylation of the fluorinated compound. Evidence was presented to indicate that the ratio of striatal to cerebellar radioactivity increased with time at approximately the same rate for both F-dopa and [^{3}H]L-dopa. A uniform distribution of OMFD was reported in both the cerebellum and the striatum (Melega et al., 1990).

Neff and Hadjiconstantinou have recently reported that AADC activity in dopaminergic neurons is modulated by physiological stimuli and by neuroactive drugs. Changes in AADC activity, in response to environmental lighting, were monitored in the rat retina, and the effects of MPTP treatment and treatment with dopamine receptor antagonists were measured in the mouse striatum. It was concluded that AADC activity is modulated by neurotransmitter receptors (Neff and Hadjiconstantinou, 1992). This information provides a crucial link between AADC activity, as measured through the administration of labelled L-dopa, and endogenous rates of dopamine synthesis, which were previously thought to be modulated only by tyrosine hydroxylase.

These studies and others have clearly contributed a great deal to current understanding of the dopaminergic system. None of the above methods, however, enable the study of dopamine metabolism in living man.

The Synthesis and Metabolism of Dopamine in the Striatum:
Positron Tomographic Studies

This laboratory first demonstrated the use of [^{18}F]6-fluoro-L-dopa (F-dopa) and positron tomography (PET) to visualize dopamine in living man in 1983 (Garnett et al., 1983). Three years later, we published a study of L-dopa metabolism in monkeys with 1-methyl-4-phenyl-1,2,4,6-tetrahydropyridine (MPTP) induced Parkinsonism. We demonstrated that ^{18}F activity measured by PET was correlated to dopamine content, tyrosine hydroxylase activity, and dopa decarboxylase activity (Chiueh et al., 1986).

In 1987, we conducted a positron tomographic study of the cerebral metabolism of F-dopa in the monkey, using F-dopa and L-[^{14}C]dopa as tracers. We found that fluorodopamine was the predominant striatal metabolite, accounting for two thirds of striatal radioactivity in the first fifty minutes following injection. We calculated the half life of striatal fluorodopamine to be approximately sixty minutes. In the plasma, striatum, and cerebellum, we found that F-dopa disappeared more quickly than L-[^{14}C]dopa, and postulated that this rapid clearance may be due to accelerated decarboxylation of the fluorine-labelled analogue. The contribution of [^{18}F]fluoro-3-O-methyl-L-dopa (OMFD) was found to account for less than ten percent of the radioactivity in the striatum at any time in the two hour study (Firnau, 1987), although this result has been subsequently challenged (see Melega et al., 1990).

The metabolism of F-dopa was further probed by Pate et al., who administered F-dopa to live rhesus monkeys in conjunction with neuroactive drugs. The administration of NSD 1015, an inhibitor of AADC, was found to reduce striatal retention of ^{18}F, as was reserpine, an inhibitor of vesicular storage. MAO inhibitors were found to have no effect on striatal uptake. In contrast with the suggestions of Reith et al., it was concluded that F-dopa metabolites were retained in the neurons during the two hour length of the study (Pate et al., 1990).

Barrio et al., compared the "cerebral kinetics and metabolism" of F-dopa in two normal monkeys and two monkeys with MPTP-induced Parkinsonism. MPTP-treated monkeys were found to have a forty to fifty percent reduction in striatal accumulation of radioactivity; compartmental analysis revealed that this reduction was attributable to an increased turnover rate for stored dopamine in surviving neurons. Evidence was presented to suggest that exogenous F-dopa is converted to fluorodopamine and stored in a "slow turnover rate functional pool", while newly synthesized dopamine from endogenous tyrosine is preferentially released and metabolized. In view of the generally accepted concepts of tyrosine hydroxylase as the rate-limiting and modulated step in endogenous dopamine synthesis, conclusions were drawn that a direct correlation between fluorodopamine synthesis and dopamine synthesis from endogenous tyrosine may not exist (Barrio, 1990).

These results were confirmed by Melega et al., of the same research group, who used data from these four monkeys to demonstrate that endogenous dopamine and dopamine metabolite concentrations were similar, while fluorodopamine concentrations were greater than those of its metabolites. It was inferred that exogenous F-dopa predominantly labels only the slow turnover rate functional pool of dopamine. Although the accumulation of [^{18}F] activity does not reflect of endogenous dopamine synthesis (since tyrosine hydroxylase has been by-passed), Melega et al. argue that this accumulation still provides an assessment of the integrity of dopaminergic neurons (Melega, Hoffman, et al., 1991).

The Distribution of O-Methyl-F-dopa --

O-methyl-F-dopa, like O-methyldopa, is formed in the blood and enters the brain, contributing to background activity in the time course of radioactivity in dopaminergic areas of the brain. The distribution of this metabolite in the brain must therefore be determined, in order to correct for the contribution of radioactivity attributable to OMFD.

To verify the assumption that OMFD is present as a homogenous distribution throughout the brain, Doudet et al. administered OMFD to normal rhesus monkeys and animals with lesions in the nigrostriatal system. No selective accumulation of

radioactivity in the brain was apparent in normal or lesioned animals. Only metabolites which do not cross the blood-brain barrier were detected in a plasma metabolite analysis. A one-compartment, three-parameter model was adequate to describe the kinetics of OMFD in the brain. This model describes a simple two-rate constant delay of the input function; the third parameter is the blood volume. The volume of distribution of OMFD in the brain was found to be close to unity. This distribution volume implies that OMFD freely diffuses throughout the water compartment of the tissue, and that this compartment comes into equilibrium with the concentration of OMFD in the plasma (Doudet, 1991). This value was confirmed by others (Melega, Grafton et al., 1991).

OMFD was also used as a tracer in monkeys by Pate et al. In this study, striatal regions of interest showed intensities indistinguishable from cortical regions of interest. The cortical regions were therefore used to estimate the background activity attributable to OMFD in the striatum after an F-dopa injection (Pate et al., 1991).

The Effect of Carbidopa Pre-treatment --

Carbidopa, a decarboxylase inhibitor, is often administered prior to an F-dopa injection, in an attempt to increase striatal uptake of the labelled molecule by decreasing peripheral metabolism. Although the effects of this "pre-treatment" have been discussed by many authors (see, for example, Garnett et al., 1983), several studies

of the use of carbidopa with F-dopa, in positron tomography, have recently appeared in the literature.

The effects of carbidopa pre-treatment on F-dopa metabolism were analyzed by Melega et al. in the rat, monkey and human. Significant increases in the metabolism of F-dopa to OMFD were found in the plasma metabolic profiles of each species after carbidopa pre-treatment. Carbidopa pre-treatment was reported to effect a seven hundred percent increase in striatal fluorodopamine, as measured in the metabolic profile of the rat brain, thirty minutes after F-dopa administration. In humans, significant increases in F-dopa plasma concentrations (between 20 and 50 percent) were maintained for thirty minutes after F-dopa injection. These investigators concluded that carbidopa pre-treatment significantly increases the amount of radioactivity in the brain that can be attributable to fluorodopamine (Melega et al., 1990).

Peripheral and cerebral F-dopa metabolism after carbidopa pre-treatment were further investigated by Melega et al., in an effort to formulate a tracer kinetic model for use with F-dopa in PET. When a sufficient dose of carbidopa is administered (200 mg, 90 minutes prior to F-dopa injection), it was found that peripheral metabolism in humans is restricted to OMFD. Thus, only OMFD and F-dopa can enter the brain from the blood (Melega, Grafton, et al., 1991). These results were used to configure the model of F-dopa metabolism described in Chapter 3 (see Huang et al., 1991).

Recent studies by Hoffman et al. confirm that carbidopa pre-treatment results in increases in plasma concentrations of F-dopa and OMFD in monkeys and humans. Total striatal and cerebellar accumulation of radioactivity, as measured by PET, also increases by up to 50 percent. Increases in specific striatal accumulation were found to correlate with increases in plasma F-dopa concentrations. It was concluded that measured increases in striatal tomographic activity were secondary to increases in plasma F-dopa concentrations, rather than the result of changes in the F-dopa influx rate constant. In light of these results, it was suggested that the main advantage of carbidopa pre-treatment is to increase striatal tomographic activity without commensurate increases in radiation dose (Hoffman et al., 1992).

Conclusions

These studies, then, have demonstrated the validity of F-dopa as a tracer for investigating the dopaminergic system in living man. It may be concluded from these results that F-dopa enters the brain and is rapidly metabolized to fluorodopamine. fluorodopamine appears to be stored in the neuronal vesicles, in a slow turnover pool, to give a biological half-life of about one hour in the striatum. While the correlation between fluorodopamine synthesis and endogenous synthesis has been questioned, recent studies indicate that the activity of AADC is modulated by physiological stimuli and neuroactive drugs (Neff and Hadjiconstantinou, 1992). The distribution of OMFD is roughly uniform throughout the brain, with a distribution volume close to unity. The

main advantage of carbidopa pre-treatment is to increase the total accumulation of radioactivity in the striatum, because of increased plasma F-dopa concentrations. However, OMFD concentrations in the plasma and in all parts of the brain are also increased by this inhibitor.

It is clear that these studies have contributed greatly to the understanding of the transport and metabolism of F-dopa in the brain. This understanding serves, in turn, as the biological framework for various mathematical models of F-dopa metabolism. These models, used in conjunction with positron tomography, are then able to provide quantitative measures of metabolic processes in life.

Chapter 3

Mathematical Modelling of PET Studies which use F-Dopa as Tracer

Although several research groups have undertaken the study of dopaminergic function with positron tomography, no definitive means of quantitatively analyzing the results of these studies has emerged. The subsequent paragraphs offer a review of important contributions to tracer kinetic modelling in general, followed by an overview of modelling techniques currently being proposed by various researchers in the field.

Tracer Kinetic Modelling

In 1981, Zierler presented a review and critique of compartmental analysis. As well as providing an overview of the historical origins of this technique, Zierler critically examined the uses and underlying assumptions of this method. Each of these assumptions is delineated in the course of a derivation, from first principles, of the general equations of compartmental analysis (see Equations 4 and 5). The assumptions include: that the system is linear; that stationarity holds; that material is neither created nor destroyed in any compartment; that the compartments are homogenous, or "well-mixed"; and that the parameters of the model, or rate constants, are truly constant with respect to time and tracer concentration. General solutions are presented for two-

compartment systems; common errors in the use of this technique, such as the violation of the above assumptions, or the collection of inadequate data, are also discussed. The use of independently-determined information in model formulation is emphasized; it is argued that this method of analysis is only appropriate in the case of physical phenomena known on independent grounds to be described by first-order linear equations. Zierler cautions against the use of this approach as "an exercise in curve-fitting", in which no physical meaning can be attributed to the mathematical solution (Zierler, 1981).

DiStephano and Landaw (1984) later reviewed the use of multiexponential, multicompartmental and noncompartmental modelling. These three approaches are compared, with the emphasis that noncompartmental analysis is *not* model independent -- for example, the graphical methods described in the first chapter of this thesis each pre-suppose a certain compartmental model. It is further emphasized that the model which best fits the data, in a statistical sense, may be simpler than the known physiological structure of the system. The optimal weights to be used in a weighted least squares minimization, the covariance matrix estimate of parameter variance, and the use of the F-test are explained in a companion article (Landaw and DiStephano, 1984).

The use of mathematical modeling in the analysis of *in vivo* neuroreceptor binding of radioligands was later reviewed by Gjedde and Wong. A synthesis of

kinetic models developed for the analysis of positron tomographic data is presented, with reference to publications between 1977 and 1987. The basic equation and basic solution for general two- and three-compartment models are provided, along with positron tomographic, autoradiographic, and normalized (referred to in this thesis as *graphical*) solutions. The rate constants determined by these methods are also derived in terms of the permeability-surface area product and perfusion, and in terms of the parameters of the Michaelis-Menten equation. The interference of labeled metabolites of the tracer is discussed. Gjedde and Wong focus on the practical estimation of a number of fundamental binding kinetic constants *in vivo*, through a variety of analytical methods (Gjedde and Wong, 1990).

Patlak et al. introduced a method of graphing multiple-time tissue uptake data in 1983. Although this approach has been detailed in the second chapter of this thesis, a synopsis will be offered here for completeness. A linear compartmental model was proposed which assumes an arbitrary number of reversible tissue compartments and one or more irreversible tissue regions. This method plots the total tissue solute concentration at the times of sampling (A_m) versus the arterial plasma concentration-time integral, both normalized to the plasma concentration at the respective times (C_p). It was shown that the graph will yield a curve that eventually becomes linear, with a slope equal to the influx constant for the system (K_i), and an ordinate intercept less than or equal to the vascular plus steady-state space of the reversible tissue region (Patlak et al., 1983). This technique was extended by Patlak and Blasberg for

situations in which the plasma concentration of the solute cannot be easily measured. In this case, a modified approach can be used in which the tissue concentration in a region with no irreversible trapping is substituted for C_p. The slope of the graph obtained by this method is equal to the influx constant divided by the sum of the steady state space and plasma space in the reversible region (Patlak and Blasberg, 1985).

This method was further modified by Logan et al., who presented a graphical method applicable to tracers for which there is no irreversible accumulation. In this method, the ratio of the concentration-time integral (up to the sampling time) for a region of interest to the concentration in the region at the sampling time (*ROI(t)*) is plotted against the ratio of the plasma concentration-time integral to *ROI(t)*. This graph will yield a curve which eventually becomes linear, with a slope equal to the vascular plus steady-state space of the tracer (Logan et al., 1990).

Modelling of F-dopa/PET studies

In 1980, this laboratory conducted a study of F-dopa metabolism in monkeys, using two gamma detectors to determine the time-course of radioactivity in the head and the blood. The blood response was fitted to the sum of two decaying exponential functions. Evidence was presented to verify that no labeled metabolites of F-dopa were present in the blood during the ten minute period of measurement. A three-

compartment model was necessary to adequately describe the time-course of radioactivity in the head. These compartments were ascribed to: blood in the vessels in the brain; intracerebral endothelial cells and their neighbouring pericytes; and neurons. In this way it way possible to derive the fractional rate constants for the forward and back flux of F-dopa between the blood and the capillary wall, for the formation of dopamine from dopa, and for the destruction of dopamine, although this last rate was found to be very slow (Garnett et al., 1980).

Itoh et al. investigated the effect of labelled metabolites on the estimation of influx constant for F-dopa in the striatum. Using high pressure liquid chromatography, plasma metabolic profiles were obtained in normal subjects after injection of F-dopa. The appearance of metabolites in the plasma was found to produce an underestimation of the F-dopa uptake rate. It was suggested that disregard for labeled metabolites in the plasma could result in a forty to sixty percent reduction in the estimated influx constant (Itoh et al., 1988).

Various means of correcting for the contribution of labeled metabolites in the plasma, and in striatal radioactivity, have been presented. Martin et al. subtract radioactivity in the posterior temporoparietal cortex from total striatal radioactivity at each time point to obtain "specific striatal activity", which is used as A_m in the graphical analysis of Patlak. To determine C_p, the time course of OMFD in the plasma is estimated through an evaluation of the ratio of OMFD to F-dopa in the plasma and

its rate of change over time. The time-course of radioactivity attributable to F-dopa in the plasma (C_p) is then calculated by subtracting the contribution of OMFD from the total plasma activity curve. It is demonstrated that with these corrections, the slope of the plot is representative of the influx of F-dopa, from the blood, to the irreversible compartment specific to the striatum. Martin et al. found an inverse linear relationship between the influx constant calculated in this manner and age (Martin et al., 1989). A simplified method for determining the time course of F-dopa in the plasma has recently been presented by this group. Because the ratio of F-dopa to labelled metabolites changes linearly with time, the measurement of this fraction in a single plasma sample, collected late in the study, is sufficient to determine the time course of F-dopa concentration in plasma (Chan, et al., 1992).

A comparison of two similar graphical approaches was conducted by Sawle et al. in another study of striatal function and aging. This study used the graphical method of Patlak, but compared the use of two different sets of variables as A_m and C_p. One method used corrections identical to those of Martin et al., except that radioactivity in the cerebellum, as opposed to the posterior temporoparietal cortex, was used as reference. A second method was also employed, in which the time-course of radioactivity in the occiput was implemented as C_p, while the total radioactivity in the striatum was used as A_m. Although no attempt was presented to compare these two approaches on theoretical grounds, a significant correlation between the influx constants derived by each method was found. Neither method of analysis demonstrated a

correlation between age and the influx constant for the caudate, putamen, or medial frontal cortex (Sawle et al., 1990).

A similar study was presented by Itoh et al., who compared the use of three different variables as input functions in the graphical method of Patlak. Using the results of plasma metabolite analysis, the fraction of F-dopa in the plasma at all times was estimated. This allowed for the calculation of the time-course of radioactivity attributable to F-dopa in arterial plasma (the "F-dopa input"). The influx constant for F-dopa uptake was calculated using total striatal radioactivity as A_m, and using F-dopa input, total plasma ^{18}F input, or the time-course of radioactivity in the cerebellum, as C_p. The mean F-dopa influx rate was calculated as 0.020 ± 0.008, 0.009 ± 0.004, and 0.012 ± 0.003 [min^{-1}] (mean ± SD), for the three methods respectively. It was concluded that the cerebellum input yielded the smallest variance in the influx constant; a large variance in the results of the F-dopa input method suggested that highly accurate assessment of the plasma metabolites is necessary. A "bi-phasic" change in F-dopa metabolism with age was reported; the influx constant appeared to increase between the ages of 30 and 55, and decreased thereafter (Itoh et al., 1990).

Hartvig et al. introduced yet another modification to this graphical analysis in a study of the kinetics of L-[β-^{11}C]dopa in humans. In this study, the time-course of radioactivity in the whole brain was substituted for arterial plasma radioactivity in the Patlak approach. The result of this substitution is examined theoretically to determine

the rate constant for brain utilization of L-dopa in terms of the slope and intercept of the plot. It is argued that this rate constant is an estimate of the rate of decarboxylation of L-dopa, while the influx constant reflects a large number of processes, such as blood-brain barrier transport, metabolism in the capillary wall, uptake into dopaminergic nerve terminals, AADC activity within the neurons, and storage in neuronal vesicles. The rate of decarboxylation of L-dopa was found to be 0.012 ± 0.005 [min^{-1}] (mean ± SD, n = 8) in the basal ganglia. A two-fold difference in this constant was observed between normal subjects (Hartvig et al., 1991).

A compartmental model which explicitly accounts for the contribution of OMFD has been used by Gjedde et al. to study dopa decarboxylase activity in man. A two-compartment, two-parameter model is first studied by a graphical technique to determine the coefficient of methylation in the plasma, and the loss of OMFD from the plasma. These values are used to construct the time course of F-dopa and OMFD in plasma. A two-compartment, five-parameter model of an extrastriatal region of the brain is then solved by regression. The number of parameters is reduced to three by assuming: that the ratio of the blood-brain barrier clearance of F-dopa (from blood to brain) to that of OMFD is constant for all subjects and equal to that value determined in previous studies of the rat (see Reith et al., 1990); and that this ratio also applies to transport from the brain to the blood. A three-compartment, seven-parameter model for the striatum is similarly reduced to three parameters, by making the above assumptions, plus the additional assumptions that: the F-dopa partition volume, V_e, is

equal in the two regions of the brain; and that there is negligible methylation of F-dopa in brain tissue. Dopa decarboxylase activity was measured by this method in ten regions of the brain, for six healthy volunteers (Gjedde et al., 1991).

This model has been recently used by Gjedde et al. to determine the rate of decarboxylation of F-dopa in normal volunteers and patients with several diseases which have been linked to abnormalities in dopaminergic transmission. The decarboxylation rate was measured in six regions of the brain for twelve healthy volunteers (0.080 ± 0.017), six patients with Parkinson's disease (0.050 ± 0.012), and five patients with schizophrenia (0.105 ± 0.019) [min^{-1}] (mean ± SD, left caudate). Significant differences were found between the normal controls and the latter two groups ($P < 0.05$) (Gjedde et al., 1992).

The kinetics of F-dopa in striatum and cerebellum were measured in ten normal human subjects by Huang et al. The time-course of arterial plasma concentrations of the tracer and its metabolites were also assayed biochemically. A two-compartment, three-rate constant model was used to describe the time-course of radioactivity in the plasma; this approach was used to separate the contributions of F-dopa and OMFD from the total plasma radioactivity. These separate contributions were then used as input functions to separate compartmental models which describe the kinetics of F-dopa and OMFD in the striatum and cerebellum. This approach resulted in a two-compartment, four-rate constant model for the cerebellum and a three-compartment, six-

rate constant model for the striatum. The use of the model for plasma time-activity data was compared to the method of fitting the plasma activity curve to a sum of decaying exponentials. Differences in the optimal model parameters of F-dopa in the striatum were found to be "extremely small" when the plasma modelling approach was replaced by this simple exponential fit. In the solution of the striatal compartmental model, one rate constant could not be uniquely determined, and therefore the ratio of two rate constants was constrained. Although the influx constant for the system (as calculated from the model parameters) did not depend upon the value chosen for this constraint, the rate constant which represents the formation of fluorodopamine from F-dopa varied linearly with this value. Statistical calculations (F test) on the model fitting indicated that the tissue kinetics were more consistent when a clearance pathway from the fluorodopamine (and metabolites) compartment in the striatum was included. Neglecting this rate constant caused a fifty percent change in the influx constant. A large inter-subject variability was reported in the rate of peripheral O-methylation of F-dopa. The rate of decarboxylation of F-dopa in the striatum was found to be 0.041 ± 0.002 [min^{-1}] (mean ± SD) (Huang et al., 1991).

To summarize, models currently in use can be broadly categorized as graphical analyses, with some simple subtraction to correct for OMFD, or compartmental analyses, which have grown increasingly complex in efforts to accurately model the known physiology of the system. This complexity has led to models which do not have unique solutions (Huang et al., 1991), or to a plethora of assumptions which

collapse the model to solvable dimensions (Gjedde et al., 1991). Although it is possible to calculate the influx constant derived by graphical analysis from the parameters determined by compartmental analysis (see Equation 17), it is worth noting at this point that none of these investigators have attempted this comparison. These two classes of mathematical methods, then, are distinct from each other; inter-class comparison is not attempted.

The Use of Modelling Techniques in Studies of Parkinson's Disease

In order to determine the clinical value of these mathematical techniques, a review of F-dopa/PET studies of Parkinson's Disease was completed.

Brooks et al. studied patients with multiple system atrophy, pure autonomic failure, and Parkinson's disease. In this study, the integrity of the striatal dopaminergic system was evaluated using a modified Patlak analysis; the time-course of radioactivity in the occipital lobe was substituted for the arterial plasma time-activity curve. While the influence of fluorodopamine clearance and OMFD background is discussed, no attempt is made to correct for these effects, since the simple graphical approach provides a reasonable means of comparing dopaminergic function between groups of patients (Brooks et al., 1990).

The same graphical method is employed by Lindvall et al. to evaluate the

survival and efficacy of fetal dopaminergic grafts. In this study, the influx constant is compared between normals and a single patient, both pre- and post-operatively (Lindvall et al., 1990).

In a study of the rate of loss of dopaminergic integrity in normal subjects and patients with Parkinson's disease, Bhatt et al. used a simple ratio of striatal to background activity to evaluate striatal uptake. This ratio was taken as the highest activity found in a pixel of the striatal region of interest, divided by the mean activity in the temporoparietal cortex. Contrary to expectation, the rate of loss of integrity of the dopaminergic nigrostriatal pathway in patients with idiopathic Parkinson's disease was found to be slow, and comparable to the rate in normal controls (Bhatt, 1991).

Tedroff et al. administered pharmacological doses of unlabelled L-dopa with [^{11}C]-labeled L-dopa to patients with Parkinson's disease, in order to evaluate the clinical effect simultaneously with the cerebral kinetics of the drug. In this study, white matter was used as the reference tissue in a graphical analysis. A significant inverse correlation was found between plasma concentrations of large neutral amino acids and the uptake of radioactivity in the white matter, indicating a competitive influence (Tedroff, 1992).

In 1992, Eidelberg presented a review of PET studies in Parkinsonism. The appeal of graphical analyses, particularly those for which a reference region in the brain

may be used (thus avoiding plasma sampling and fractionation) is acknowledged; the possibility of separately determining transport and decarboxylation rate constants through compartmental analysis is also mentioned. Referring to the contradictory results of Martin (1989) and Sawle (1990), the unresolved issue of striatal function in normal aging is discussed. Eidelberg comments that "controversies in this area may be rooted in the diverse methodological approaches employed in the estimation of F-dopa uptake rate constants which are presently unresolved" (Eidelberg, 1992).

In summary, only simple ratios or graphical analyses are being used in clinical studies of Parkinson's disease, and even so the diversity of approaches has confounded efforts to answer some of the most basic questions. The numerical values of the influx constants calculated by various research groups cannot be compared, because of the vastly different assumptions and methodologies employed. Although the influx constant may provide a means of comparing groups of patients or normals, it is influenced by a number of physiological processes, and provides no indication of which of these processes might be accelerated or impaired. There is a tremendous need for a modelling approach which will offer a more informative means of comparing individuals, and disease states, without over-determination.

Chapter 4

Modelling F-dopa Metabolism in the Living Brain -- A New Approach

Introduction

In light of the controversies surrounding the mathematical modelling of positron tomographic studies with F-dopa as tracer, a sound methodological approach to model derivation must be adopted. If compartmental analysis is to be used, models of increasing complexity must be evaluated, using statistical methods, to determine the simplest model which adequately fits the measured data. *This is the only model which is mathematically justifiable.* If graphical analysis is to be used, care must be taken to ensure that any corrections that are made to the data are both mathematically and physiologically justifiable. Lumped parameters, such as the influx constant, are generally less sensitive to noise in the measured data, and are valuable in comparing groups of individuals; compartmental analysis, however, can provide a number of informative parameters for each individual studied. It would be valuable, therefore, to perform both types of analysis, and to derive the mathematical expression which relates the results of the two. In this way, the results can serve as an internal standard, a measure of the integrity of the analysis as a whole.

Experimental Protocol

With these considerations in mind, an analysis of fourteen F-dopa/PET studies was undertaken. After a bolus injection of between 5 and 10 mCi of F-dopa (with a specific activity of 2 Ci/mM), subjects were scanned for 12 frames at 10 seconds per frame, 6 frames at 30 seconds per frame, and 23 to 29 frames at 300 seconds per frame, for a total of 2 to 2.5 hours per study. Two of the fourteen studies were extended to 4 hours. Arterialized venous blood samples (5 to 10 ml) were taken throughout each study according to the following protocol: every 10 seconds for the first 2 minutes; at 3,4,5,7.5,10,12.5 and 15 minutes; at 20,25,30,40,50, and 60 minutes; at 75,90,105 and 120 minutes; every 30 minutes thereafter. These samples were centrifuged, and radioactivity in the plasma was counted in a well-counter, which has been calibrated to the PET scanner, and decay-corrected to the time of injection. These counts were corrected for injected dose, and expressed as a percentage of injected counts per minute.

Regions of interest were defined around the left striatum, the right striatum, and the cerebellum, which represents a non-dopaminergic area of the brain (see Figures 3 and 4). The time-course of radioactivity, expressed in counts per second per pixel, was calculated for each region. For most subjects, the average of left and right striatum at each time point was taken. Using the calibration factor between the well-counter and the tomograph (9.4×10^{-8} (counts per second per pixel) per (counts per minute per

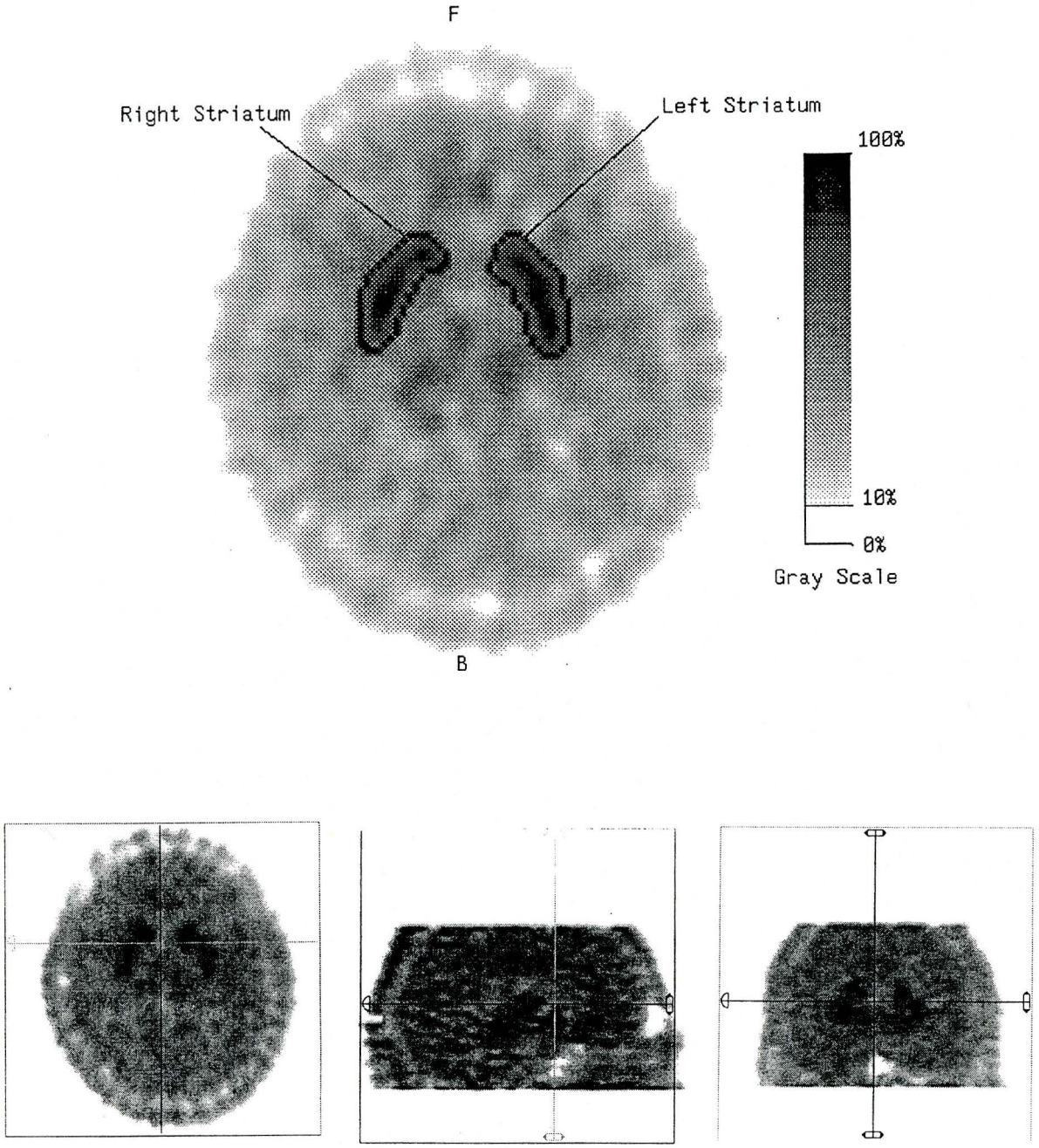

Figure 3: Accumulation of radioactivity in the brain 60 minutes after an F-dopa injection, shown in axial section through the striatum. Regions of interest are outlined; the gray scale is as shown. Sagittal and coronal sections are also provided for reference.

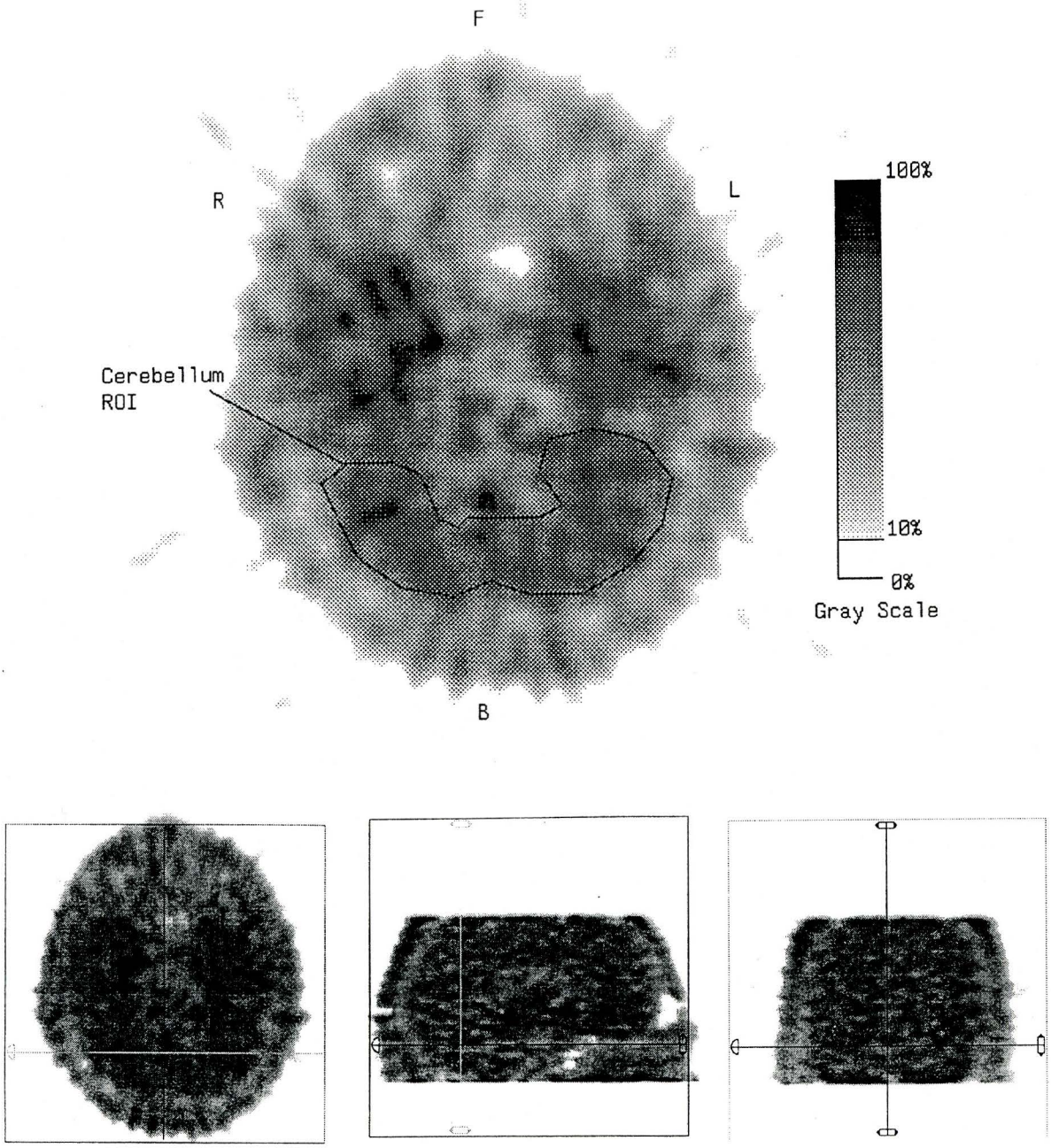

Figure 4: Accumulation of radioactivity in the brain 60 minutes after an F-dopa injection, shown in axial section through the cerebellum. The region of interest is outlined; gray scale is as shown. Sagittal and coronal sections are provided for reference.

ml)), these counts were also corrected for dose injected, and expressed in the same units as the time-activity curve for the plasma.

It was determined that the results of both compartmental and graphical analyses were sensitive to the shape of the plasma curve at early times (see "Sensitivity Analyses", below). For this reason, a fourth region of interest was defined around the posterior part of the superior venous sinus. Although the bolus has already been somewhat delayed and dispersed as it reaches the venous sinus, the time of peak radioactivity in this region, usually around 45 seconds after the start of the injection, was taken as a reasonable estimate of the time of peak radioactivity in the blood feeding the brain. To correct for delay between the blood feeding the brain and the arterialized venous samples, the peak in the blood curve was set at this time point. The peak height was set to be equal to the injected dose divided by the plasma volume of the individual, which was estimated at 35 ml/kg body weight. Sampled points were then fit to the sum of three decaying exponentials. By dividing the dose injected (counts per minute) by the y-intercepts of these exponential functions (counts per minute per ml), estimates of the volumes of three wash-out pools in the blood can be determined. These volumes and their corresponding half-lives are given in Table 1. The average percent error between the fitted and measured points, after the peak, was usually between 1 and 2 percent.

TABLE 1

VOLUMES AND HALF-LIVES OF COMPARTMENTS IN EXPONENTIAL FIT TO THE TIME-COURSE OF RADIOACTIVITY IN PLASMA.

Study Number	Volumes (l) 1st	2nd	3rd	Half-lives (min) 1st	2nd	3rd
1	2.7	34.1	84.3	0.36	3.6	101.0
2	2.7	45.1	100.0	0.34	7.9	150.3
3	2.2	20.6	55.4	0.20	2.7	61.8
4	3.0	20.3	45.7	0.29	6.8	163.5
5	4.2	51.3	99.6	0.37	8.5	162.2
6	2.4	62.6	62.6	0.07	3.0	49.1
7	2.4	40.6	78.4	0.27	5.2	159.0
8	3.9	33.5	59.8	0.34	3.3	69.5
9	2.5	62.8	84.0	0.12	4.7	103.7
10	2.0	35.4	70.8	0.20	6.5	131.2
11	3.1	52.0	91.7	0.22	12.0	102.4
12	3.8	34.2	75.6	0.07	1.6	74.0
13	2.7	24.8	61.9	0.29	3.3	94.4
14	2.9	31.1	47.8	0.12	1.3	84.5
mean	2.9	39.2	72.7	0.23	5.0	107.6
SD	0.7	13.9	17.9	0.11	3.0	39.3
%SD	22.7	35.6	24.6	45.6	59.8	36.5

Model Derivation

Compartmental Analysis

Using the time course of radioactivity in the plasma as an input function, a compartmental analysis procedure was implemented. The differential equations for the model were integrated using 4th and 5th order Runge-Kutta-Fehlberg numerical methods

(The MathWorks, Inc., 1990, pp. 137-139; Press et al., 1986, pp. 550-559). The impulse response of the model was then convolved with the plasma time-activity curve. Weighted least squares optimization of the rate constants was performed using an implementation of the Nelder-Meade simplex algorithm (The MathWorks, Inc., 1990, pp. 79-80; Press et al., 1986, pp. 289-293); the inverse of the measured values at each point were used as weights. Progressively more complex models were solved and evaluated by an F-test, under the null hypothesis that the lower-order model produced a statistically better fit. All of these numerical procedures were implemented using MATLAB software; the code for these routines is provided in the appendix.

It was found that a one-compartment, two-parameter model (Figure 2; the differential equation for this model is given in Equation 20) was sufficient to model the time course of radioactivity in the cerebellum. The inclusion of additional rate constants or compartments did not significantly improve the fit to the measured data ($F(2,50) = 2.642$, $P > 0.05$). Similarly, a two-compartment, three-parameter model (Figure 1, Equation 12) yielded the best fit to the striatal time-activity curve ($F(2,50) = 0.0996$, $P > 0.2$). Figures 5 and 6 show typical results for the compartmental analysis, for cerebellum and striatum respectively.

These results indicate that the data will not support more complex models, such as those that are used to correct for the contribution of OMFD. Additional rate constants or compartments which are necessary to make this correction are not

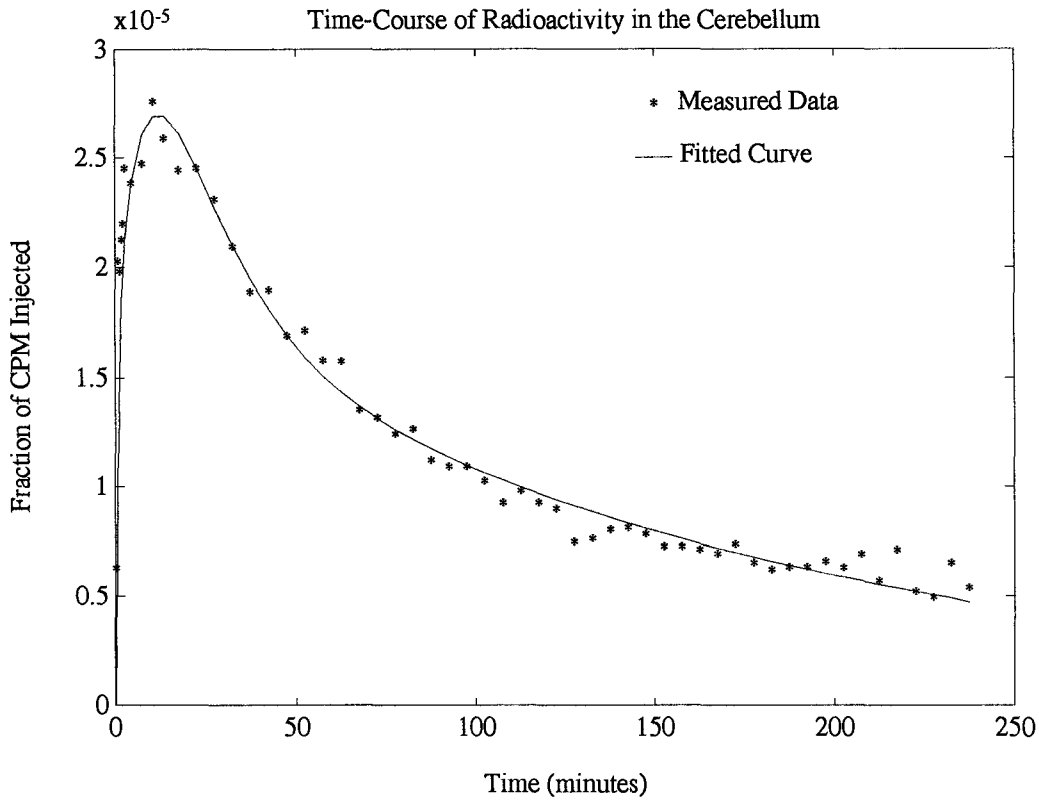

Figure 5: Time-course of radioactivity in a region of interest defined around the cerebellum; results of compartmental analysis are shown as the solid line.

mathematically justifiable with the given data. In the absence of simplifying assumptions, which effectively collapse the system to a three-parameter model (see Gjedde et al., 1991), the model will be over-determined (for example, Huang et al., 1991).

The average percent error between the fitted and measured points ranged between 5 and 10 percent for the fourteen studies. This suggests that random measurement errors or physiological fluctuations contribute from 5 to 10 percent "noise"

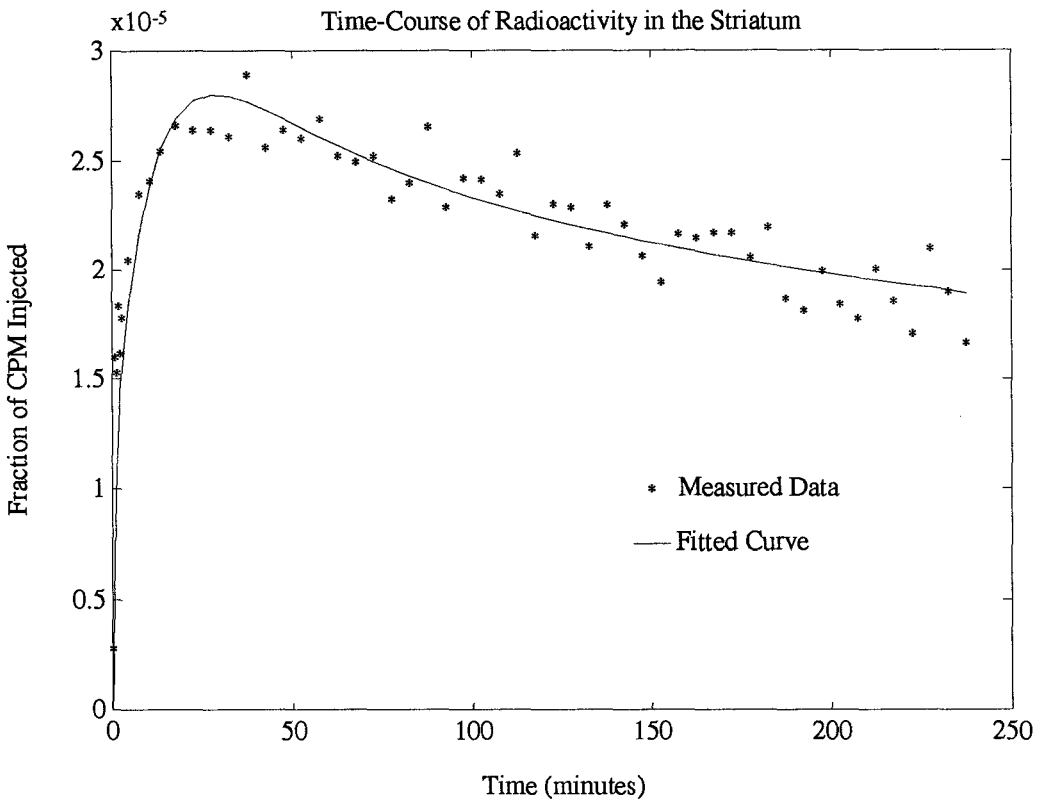

Figure 6: Time-course of radioactivity in a region of interest defined around the left and right striatum; results of compartmental analysis are shown as the solid line.

to the data measured by the tomograph (see "Sensitivity Analyses", below). This is five times greater than the random fluctuations in data recorded for the plasma.

Graphical Analysis

Since the compartmental model which best fit the measured data in the cerebellum consisted of one reversible compartment, the graphical analysis of Logan was used. This method yields a measure of the distribution volume of the tracer (and

its labelled metabolites) in the region of interest. To verify that there was no irreversible accumulation in the cerebellum, Patlak-plots of this region were also constructed. The intercepts of these plots provided verification of the distribution volume. Typical Logan- and Patlak-plots for this region appear in Figures 7 and 8.

Since the compartmental model which best fit the measured data in the striatum contained an irreversible region, the graphical analysis of Patlak was used. This

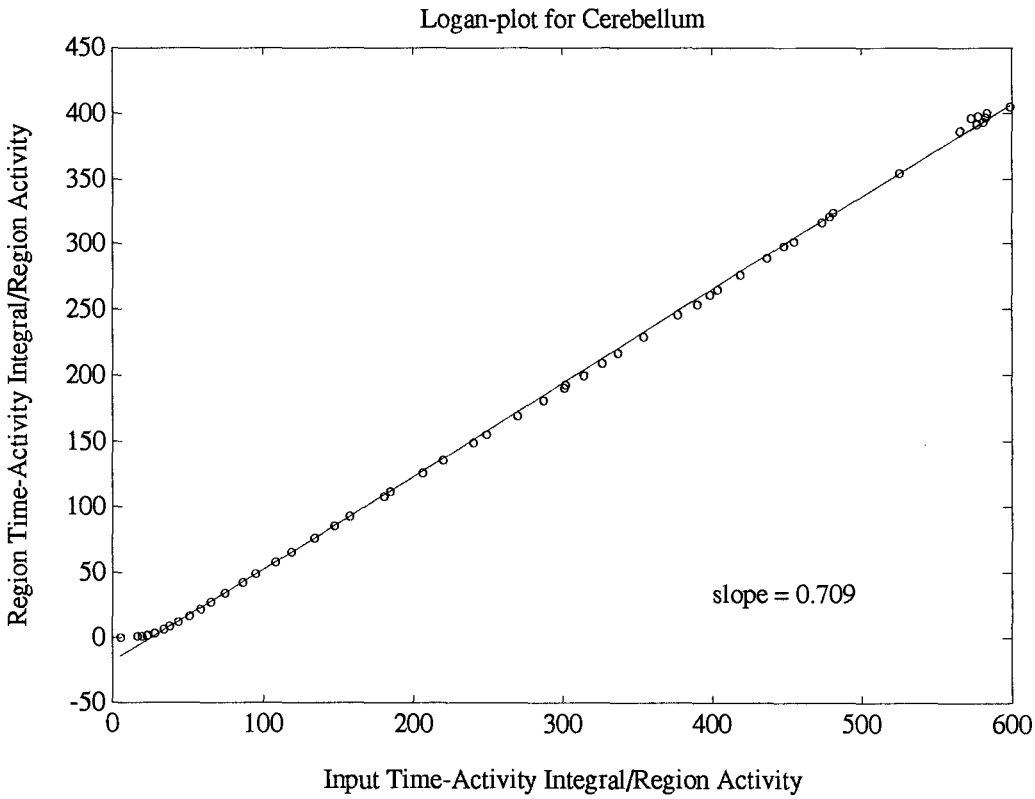

Figure 7: A Logan-plot for the cerebellum, after an F-dopa injection. The axes variables are as described in equation 22; the input function is the time-course of radioactivity in plasma.

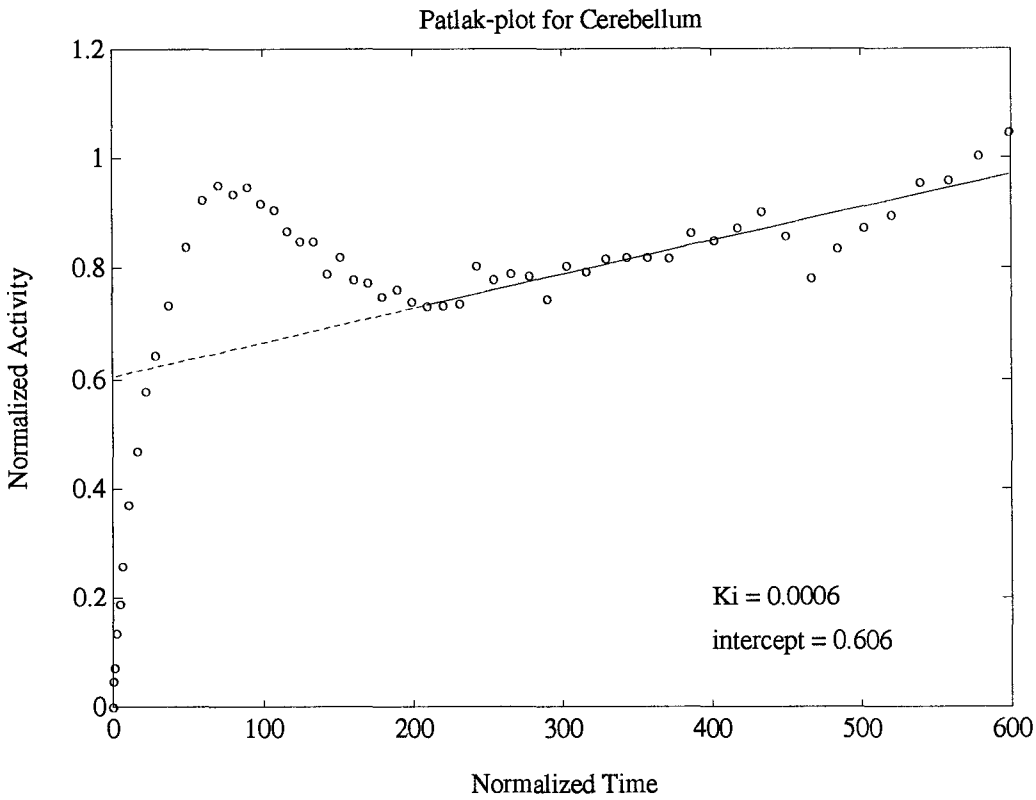

Figure 8: A Patlak-plot for the cerebellum, after F-dopa injection. Axes variables are as described in equations 18 and 19. The solid line indicates the section of the curve included in the linear regression. Note that K_i is close to zero.

method yields a measure of the net flux of the tracer into the irreversible compartment. To verify the existence of this irreversible accumulation, Logan-plots for the striatum were also constructed. These graphs should be non-linear, with slopes greater than one, if irreversible accumulation is present. Typical Logan- and Patlak- plots for the striatum are shown in Figures 9 and 10 respectively.

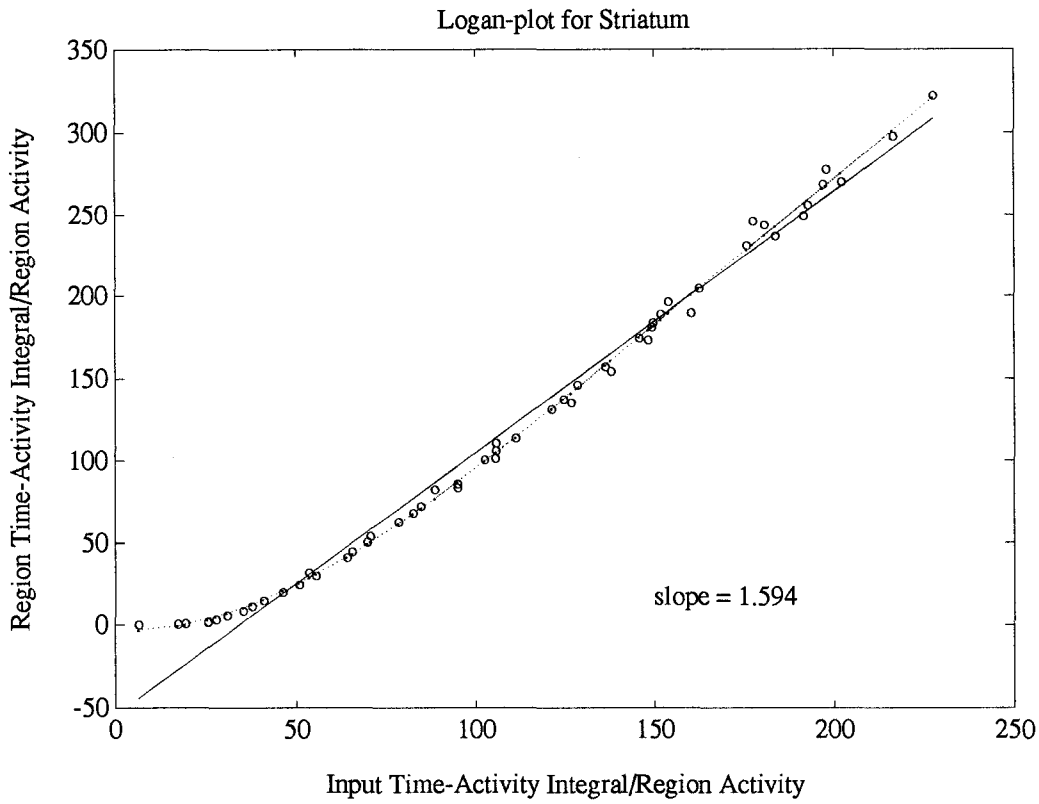

Figure 9: A Logan-plot for the striatum, after F-dopa injection. The axes variables are as described in equation 22; the input function is the time-course of radioactivity in plasma. Note that experimental points appear to follow a curvilinear function.

In this derivation of a graphical analysis for the time-course of radioactivity in the striatum, Patlak's original method, unmodified, has been implemented. An advantage of this method is that the uncorrected influx constant may be calculated in terms of the parameters of the simple two-compartment model used for the striatum, as shown in equation 17. Inter-subject comparison of this constant assumes that differences in the rate of O-methylation between individuals do not effect the results

significantly. Many investigators, however, have attempted to analyze the time course of radioactivity in the striatum using a modified Patlak approach, in order to account for background activity due to OMFD. One or more of the following corrections are often made: radioactivity measured in a non-dopaminergic area is subtracted from radioactivity in the striatum to obtain the time course of *specific striatal activity*; the time course of radioactivity in the non-dopaminergic area of the brain is used as the input function, C_p, in the graphical analysis; or the time course of radioactivity in the plasma which is attributable to labelled metabolites is subtracted from the plasma activity curve to obtain the time course of F-dopa in the plasma. The implications of using each of these three methods of correction will be discussed in turn.

Specific Striatal Activity --

In order to investigate the validity of calculating *specific striatal activity*, the time course of radioactivity in the blood and the brain after an intravenous injection of OMFD was studied in two normal individuals. Approximately 6 mCi of OMFD (with a specific activity of 2 Ci/mM) was administered in each case; the data accumulation protocol was identical to that used in F-dopa. Figure 11 shows the time-activity curves obtained one such study, for the striatum and the cerebellum. A single, reversible compartment (Figure 2) produced the best fit to the measured data. Note that the cerebellum curve is consistently higher at the beginning of the study, but drops off more quickly than the striatum in the second hour. In an F-dopa study, subtraction

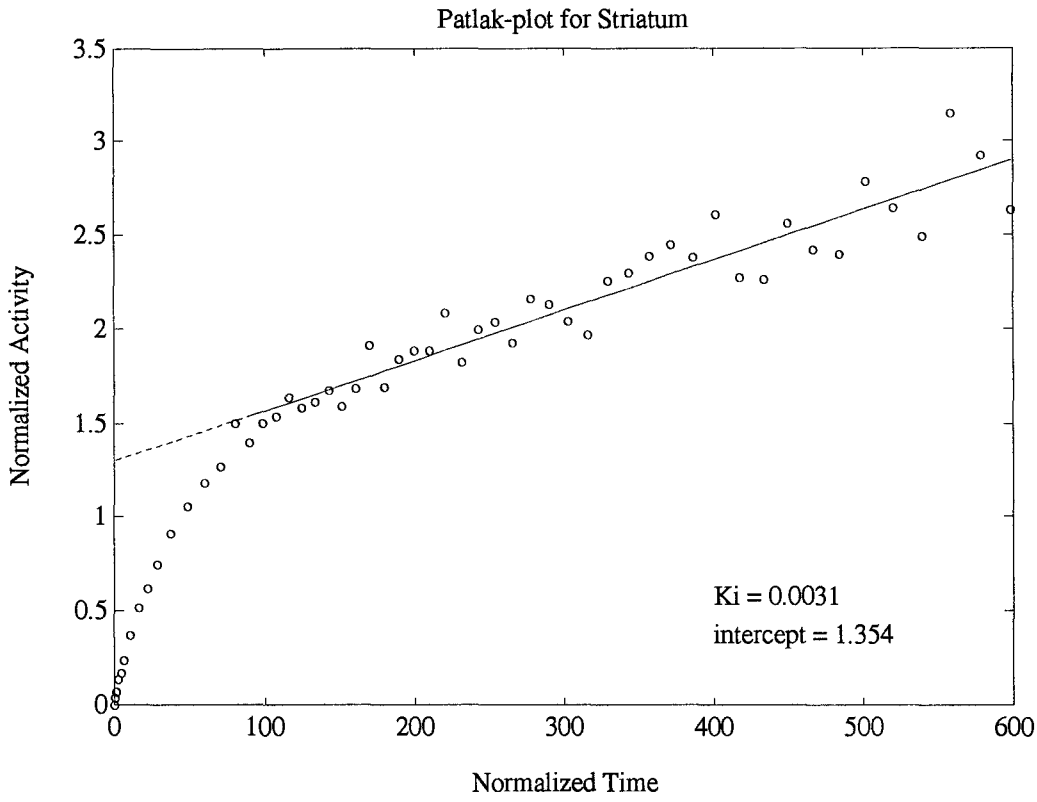

Figure 10: A Patlak-plot for the striatum, after F-dopa injection. Axes variables are as described in equations 18 and 19. The solid line indicates the section of the curve that was included in the linear regression.

of the time course of radioactivity in the cerebellum will therefore over-correct for OMFD in the first portion of the striatal curve, and under-correct later points. This will result in an over-estimation of the influx and retention of the tracer in the striatum.

These results indicate some of the problems inherent in computing *specific striatal activity*. The accuracy of the estimated influx constant can be undermined by differing time courses of background radioactivity in the striatum and the reference

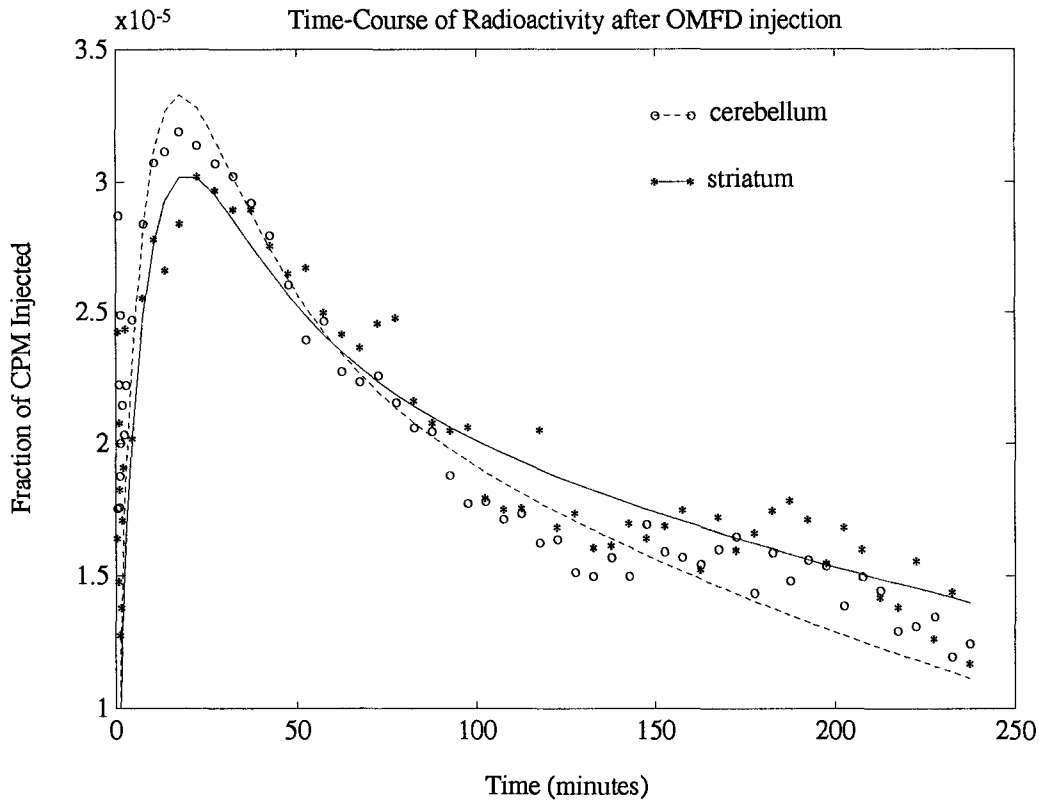

Figure 11: Time-course of radioactivity in the striatum and in the cerebellum after injection with OMFD; results of compartmental analysis are shown as solid and dashed lines.

region, while the subtraction of one noisy curve from another greatly reduces the precision of the measured values.

Non-dopaminergic Input Function --

Recall that this graphical method, as formally derived by Patlak et al. (1983), was extended by Patlak and Blasberg (1985), so that the concentration of the solute in

a region with no irreversible binding could be used as the input function, C_p. This method does *not* assume that the time-course of radioactivity in the reversible compartments for the two regions are equal. The slope of the graph in this case is equal to the influx constant divided by the sum of the distribution volume and plasma volume in the reversible area of the brain.

This graphical method does not necessitate sampling and fractionation of the blood, and it provides a reasonable measure for comparison between individuals, assuming only that the distribution and plasma volumes of the reference region are constant between subjects. Our data indicate that this assumption is reasonable (see Table 2). The random noise in the data measured by PET, however, is once again a limiting factor. Both ordinate and abscissa are normalized to $C_p(t)$ at every time point, so that random fluctuations in this curve severely undermine the precision of the plot. Since, as mentioned above, the average percent error in PET data appears to be five times greater than the error in the blood curve, noise in the non-dopaminergic input function poses a significant limitation to this method.

OMFD Contribution Subtracted from Input Function --

The formal derivation of the Patlak plot allows for any number of reversible compartments, which may be fed in series or in parallel by the blood. Conceptually, a set of compartments can be associated with the kinetics of OMFD in the brain, in

parallel to those associated with F-dopa. Material can transfer between the blood and any of these reversible compartments, without invalidating the assumptions of the derivation. If the total time course of radioactivity in the blood is considered as the input function, labelled material may flow through these parallel, reversible pathways, and into the irreversible compartment, presumably, through the F-dopa pathway only. The Patlak plot for this system will reflect the irreversible accumulation of the radio-label in the region of interest. This uncorrected influx constant will be equal to the rate of flux across the system and into the irreversible compartment, divided by the concentration of the radio-label in the source solution.

When the concentration of ^{18}F in the plasma is corrected for the radioactivity attributable to OMFD, the influx constant is theoretically equal to the rate of flux across the compartmental system and into the irreversible compartment, divided by the concentration of F-dopa in the source solution. This influx constant will differ from the uncorrected value, but both methods of analysis are consistent with the assumptions of the Patlak model.

Results and Conclusions

The results of compartmental and graphical analyses of the fourteen F-dopa studies are given in Tables 2 (cerebellum) and 3 (striatum). Studies 1 and 2 are repeat studies in the same (normal) individual; in each of these studies, scans were taken for

TABLE 2

RESULTS OF COMPARTMENTAL AND GRAPHICAL ANALYSES FOR THE CEREBELLUM, AFTER F-DOPA INJECTION.

Study Number	K_1 (ml/min/ml)	k_2 (min^{-1})	k_3* (min^{-1})	V_e** (ml/ml)
1	0.0471	0.0610		0.770
2	0.0392	0.0556		0.709
3	0.0360	0.0567		0.676
4	0.0378	0.0559		0.676
5	0.1230	0.1642		0.731
6	0.1110	0.2280	0.0024	0.590
7	0.0592	0.0936		0.621
8	0.0620	0.0897		0.697
9	0.0668	0.1064	0.0012	0.628
10	0.0393	0.0550		0.715
11	0.0529	0.0824		0.613
12	0.1021	0.1553		0.657
13	0.0224	0.0818		0.277
14	0.0944	0.1375		0.681

*k_3 was added when an additional irreversible compartment was necessary to fit the data.
**V_e refers to the distribution volume of the tracer, as determined graphically, from the slope of a Logan-plot.

four hours after the injection. The results of compartmental and graphical analyses performed on only the first two hours of these studies are also provided for comparison (see Table 4). Study 3 is a second normal individual; study 4 is a normal pre-treated with carbidopa. Studies 5 through 8 are schizophrenic patients on neuroleptic medication. Because of difficulties encountered in obtaining blood samples from patient 7, an average plasma activity curve, fitted to the measured data in twelve of the other studies, was used (the study with carbidopa pre-treatment was not included in this fit). Patient 8 was studied during the final week of a month-long "slow release"

TABLE 3

RESULTS OF COMPARTMENTAL AND GRAPHICAL ANALYSES FOR THE STRIATUM, AFTER F-DOPA INJECTION.

Study Number		K_1 (ml/min/ml)	k_2 (min^{-1})	k_3 (min^{-1})	$K_{i,c}^{*}$ (min^{-1})	$K_{i,g}^{**}$ (min^{-1})
1		0.0391	0.0309	0.0028	0.0032	0.0031
2		0.0342	0.0287	0.0028	0.0030	0.0027
3		0.0292	0.0341	0.0059	0.0043	0.0044
4		0.0342	0.0263	0.0018	0.0021	0.0024
5		0.0632	0.0998	0.0116	0.0066	0.0062
6		0.0551	0.0920	0.0080	0.0044	0.0049
7		0.0470	0.0595	0.0041	0.0030	0.0027
8		0.0383	0.0379	0.0021	0.0020	0.0019
9	r.striatum	0.0487	0.0773	0.0054	0.0032	0.0032
	l.caudate	0.0345	0.0546	0.0044	0.0026	0.0029
	l.putamen	0.0435	0.0762	0.0023	0.0013	0.0016
10	l.striatum	0.0270	0.0311	0.0031	0.0025	0.0022
	r.caudate	0.0244	0.0271	0.0031	0.0025	0.0026
	r.putamen	0.0242	0.0326	0.0012	0.0008	0.0004
11		0.0195	0.0211	0.0007	0.0006	0.0008
12		0.0482	0.0699	0.0048	0.0031	0.0031
13		0.0161	0.0322	0.0011	0.0010	0.0010
14		0.0707	0.0898	0.0058	0.0043	0.0042

*$K_{i,c}$ refers to the influx constant calculated from the compartmental rate constants.
**$K_{i,g}$ refers to the influx constant determined graphically.

neuroleptic medication. Studies 9 and 10 are hemi-parkinsonian patients; in these images, regions of interest were defined and analyzed for the whole striatum on the less afflicted side, and for the caudate and putamen separately on the more afflicted side. Studies 11 through 14 were performed for a variety of clinical reasons; subject 14 is believed to be normal.

The Cerebellum

Good reproducibility was found between repeated studies of the same individual, and between normal individuals, for both types of analysis. The percent difference between the parameters of studies 1 and 2 was less than 20 and 10 percent for the compartmental and graphical analyses respectively (K_1, 18.3%; k_2, 4.7%; V_e, 8.2%). Between the average of these two studies and the parameters for the second normal individual, percent differences were similar (K_1, 18.0%; k_2, 2.7%; V_e, 9.2%). Wide variation was found, however, between the rate constants for patients and normals. When all fourteen studies are included, the mean and standard deviation for K_1 are 0.0638 ± 0.0315 (49% standard deviation). Estimates of the distribution volume of the tracer, however, have a smaller variance; the mean value of $V_{e,g}$ is 0.646 ± 0.117 (18% standard deviation). When the distribution volume for study 13 is discarded as an outlier, the standard deviation is reduced to 7.6%. In two studies of patients, an irreversible compartment had to be added to the model to adequately fit the data.

The Striatum

Once again, good reproducibility was demonstrated between studies 1 and 2, with both compartmental and graphical parameters differing by less than 14%.

Between the average of these studies and study 3, K_1 and k_2 differed by 22.6% and 13.5% respectively. A 71% difference in k_3, however, was observed, and a 41% difference in the graphical influx constant. Since the second normal subject was approximately 25 years younger than the first, this difference could be associated with physiological, rather than methodological, causes.

Wide variation was again found between the values of the rate constants for the fourteen individuals. However, significant increases in k_3, $K_{i,c}$ and $K_{i,g}$ were observed in studies 5 and 6, patients taking neuroleptic medication. Likewise, significant decreases were observed in the influx constants for the more afflicted putamen of both Parkinsonian patients. This suggests that both compartmental and graphical analyses are able to reveal and quantify changes in the dopaminergic metabolism of individuals.

The correlation coefficient, r, has been calculated between k_3, $K_{i,c}$ and $K_{i,g}$. Between k_3 and $K_{i,c}$, $r = 0.946$, indicating that the influence of the other two rate constants in the calculation is negligible. Between k_3 and $K_{i,g}$, $r = 0.823$; for $K_{i,c}$ and $K_{i,g}$, $r = 0.825$. Thus, there is a very strong correlation between each of these measures ($t_{16} = 11.64$, 5.80 and 5.84; $P < 0.001$ in all three cases).

Table 4 gives the results of the analyses of only the first two hours of the two four-hour studies, numbers 1 and 2 in Table 3. The percent difference between the

TABLE 4:

RESULTS OF COMPARTMENTAL AND GRAPHICAL ANALYSES OF INITIAL TWO HOURS VERSUS ENTIRE FOUR HOURS OF F-DOPA STUDIES.

Study Number	K_1 (ml/min/ml)	k_2 (min^{-1})	k_3 (min^{-1})	$K_{i,c}^{*}$ (min^{-1})	$K_{i,g}^{**}$ (min^{-1})
1 (4 hours)	0.0391	0.0309	0.0028	0.0032	0.0031
(2 hours)	0.0389	0.0312	0.0027	0.0031	0.0015
2 (4 hours)	0.0342	0.0287	0.0028	0.0030	0.0027
(2 hours)	0.0342	0.0287	0.0030	0.0032	0.0032

*$K_{i,c}$ refers to the influx constant calculated from the rate constants.
**$K_{i,g}$ refers to the influx constant determined graphically.

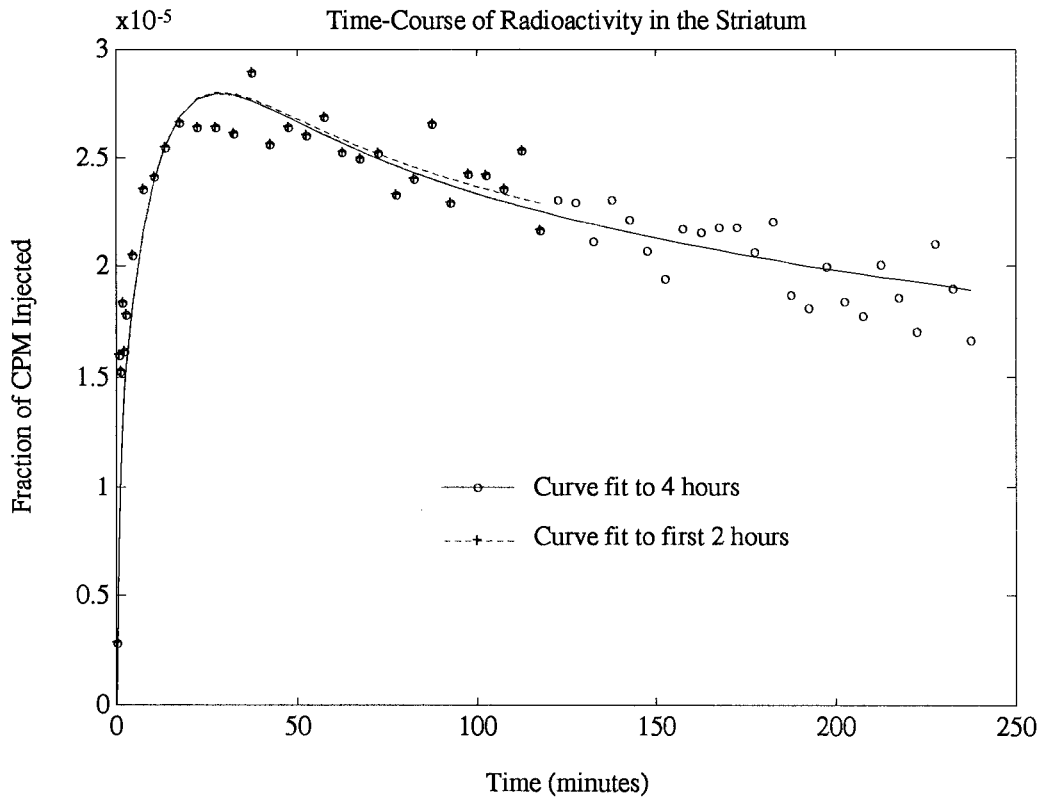

Figure 12: Time-course of radioactivity in the striatum, and the results of compartmental analysis. Curves were fit to measured data from the entire 4 hour scan; a second fit was obtained using data from the first 2 hours only.

compartmental rate constant estimates for two- and four-hour analyses are less than 1% for all cases except k_3, for which the largest difference recorded was 6.8%. Since this difference is less than 1.5 times the covariance of this parameter (see Table 8), these results indicate that a two hour study is sufficient to determine the parameters of compartmental analyses. The results of the compartmental analysis of the two- and four-hour intervals are illustrated in Figure 12. Note that the influx constant determined graphically ($K_{i,g}$) differs by over 50% when only the first two hours of the first study are analyzed. Figure 13 illustrates the sensitivity of the graphical analysis

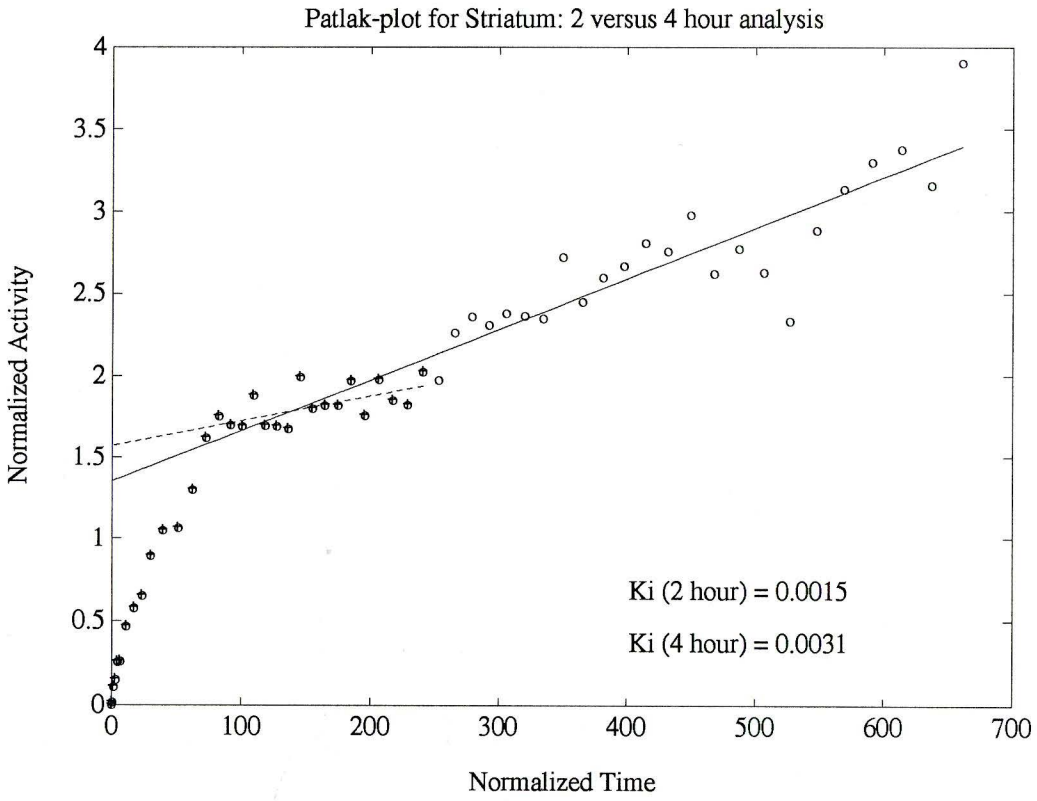

Figure 13: Patlak-plot of striatal time-activity data for Study 1, analyzed for the entire 4 hour scan time and for the first two hours only.

at the two hour mark, when the linear portion of the curve occupies only about half of the x-axis. This result suggests that the results of graphical analysis alone may be misleading if an F-dopa study is terminated 2 hours after injection.

In one study of a normal control, the time course of radioactivity in the left and right striatum were analyzed separately. Table 5 shows the results of compartmental and graphical analyses for these studies; the results of the compartmental analysis for both sides of one study are illustrated in Figure 14. The close agreement,

TABLE 5

RESULTS OF COMPARTMENTAL AND GRAPHICAL ANALYSES FOR THE LEFT AND RIGHT STRIATUM, AND FOR THE AVERAGE OF LEFT AND RIGHT STRIATUM, AFTER F-DOPA INJECTION.

Region of Interest	K_1 (ml/min/ml)	k_2 (min^{-1})	k_3 (min^{-1})	$K_{i,c}^{*}$ (min^{-1})	$K_{i,g}^{**}$ (min^{-1})
Left Striatum	0.0341	0.0278	0.0030	0.0034	0.0034
Right Striatum	0.0344	0.0292	0.0029	0.0031	0.0035
Left and Right Striatum	0.0342	0.0287	0.0028	0.0030	0.0027
Maximum % Difference	0.58	3.14	6.66	13.3	33.3
%SD(cov)†	1.13	1.36	4.66		

*$K_{i,c}$ refers to the influx constant calculated from the rate constants.
**$K_{i,g}$ refers to the influx constant determined graphically.
†SD(cov) is the standard deviation of the parameters determined from the covariance matrix; these are provided for reference.

as illustrated by percent differences which are less than 3 times the parameter standard deviations, demonstrates that no significant differences between the left and right sides of normal individuals become apparent in these analyses.

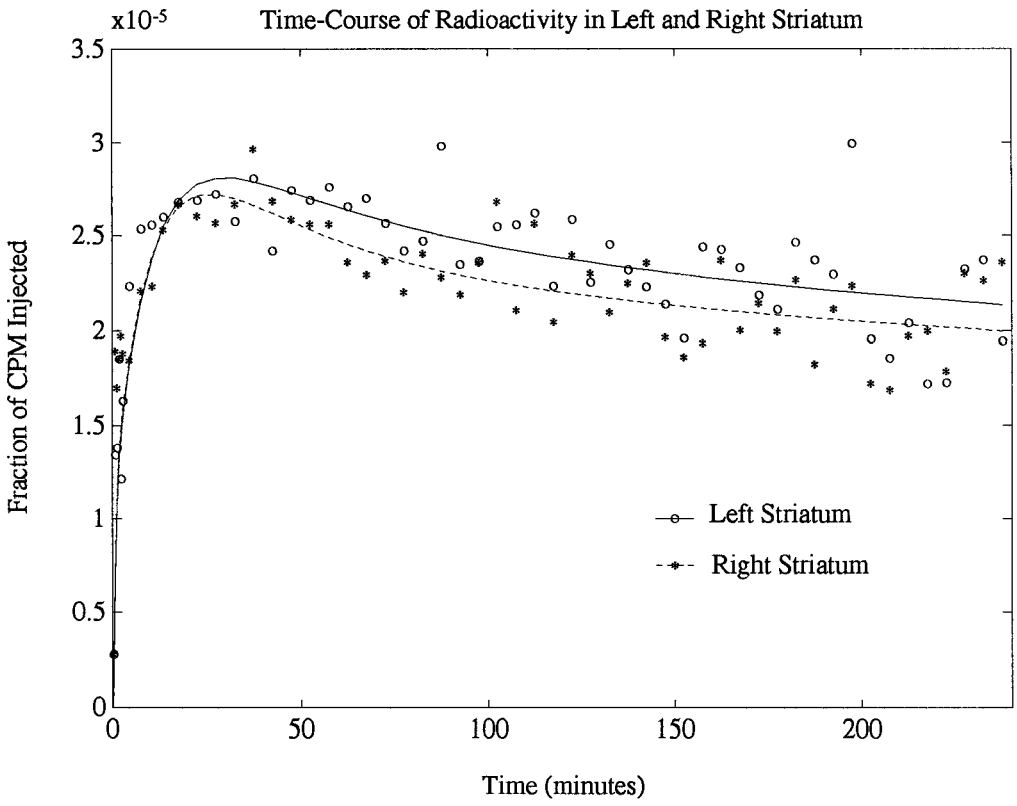

Figure 14: Time-course of radioactivity in the striatum, after F-dopa injection. Measured points and fitted curves are shown separately for the left and right striatum.

TABLE 6

RESULTS OF COMPARTMENTAL ANALYSIS AFTER OMFD INJECTION: CEREBELLUM AND STRIATUM

Study		K_1 (ml/min/ml)	k_2 (min^{-1})	K_1/k_2 (dimensionless)
A	cerebellum	0.0468	0.0470	0.996
	striatum	0.0379	0.0364	1.041
B	cerebellum	0.0455	0.0430	1.058
	striatum	0.0336	0.0299	1.124

The Distribution of OMFD

As shown in Table 6, a one-compartment two-parameter model was adequate to fit the time course of radioactivity in both the cerebellum and the striatum after OMFD injection. The two OMFD studies are once again in good agreement with each other (maximum percent difference of 19.6%). Patlak plots yielded slopes close to zero; Logan plots gave slopes close to 1. This is in agreement with the results of other investigators, who have reported no selective accumulation of OMFD in the brain, and a distribution volume close to unity (Doudet et al., 1991, Pate et al., 1991).

The Effect of Carbidopa Pretreatment

Figure 15 shows the results of compartmental analyses of striatal and cerebellar time-activity curves, for a normal individual studied with and without carbidopa

pretreatment (200 mg, 30 minutes before F-dopa injection). The difference between the striatal and cerebellar counts is plotted for each case in Figure 16. Carbidopa pre-treatment increases this difference by a maximum of about 15% of the peak height in the striatum; that is, the specific increase in striatal accumulation, relative to increases in other regions of the brain, is at most 15%.

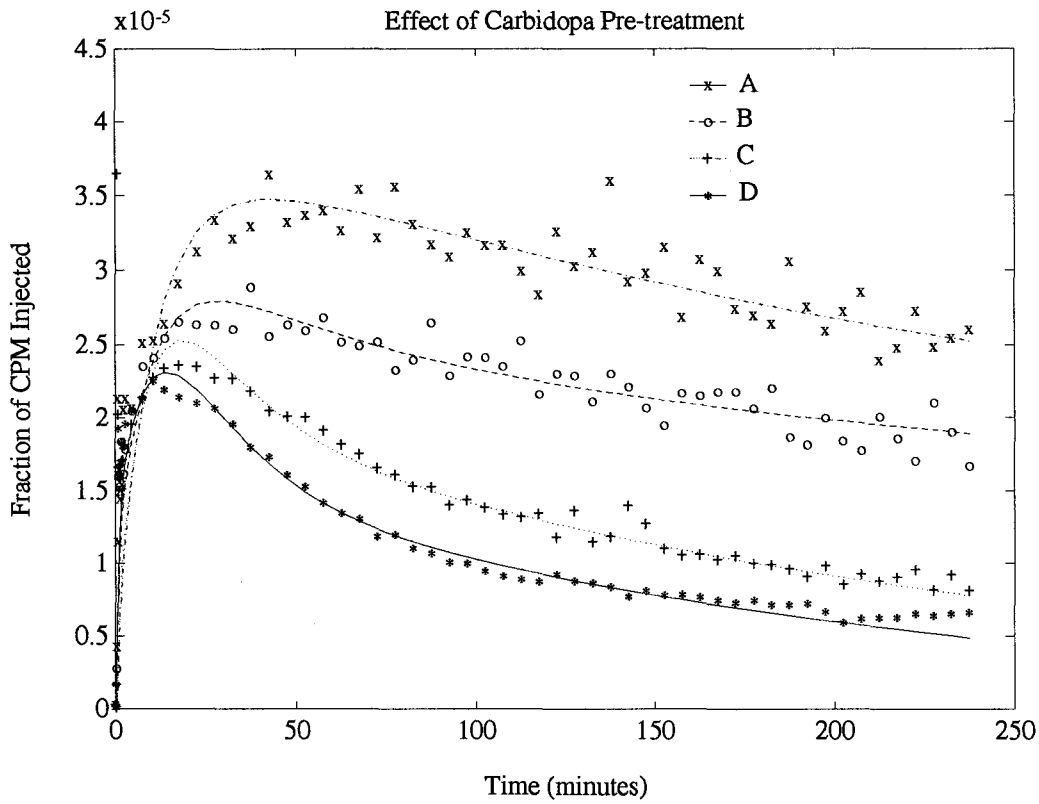

Figure 15: The effects of carbidopa pre-treatment. Curve A represents the time-course of radioactivity in the striatum, with carbidopa pre-treatment; B, the striatum without carbidopa; C, the cerebellum with carbidopa; D, the cerebellum without carbidopa.

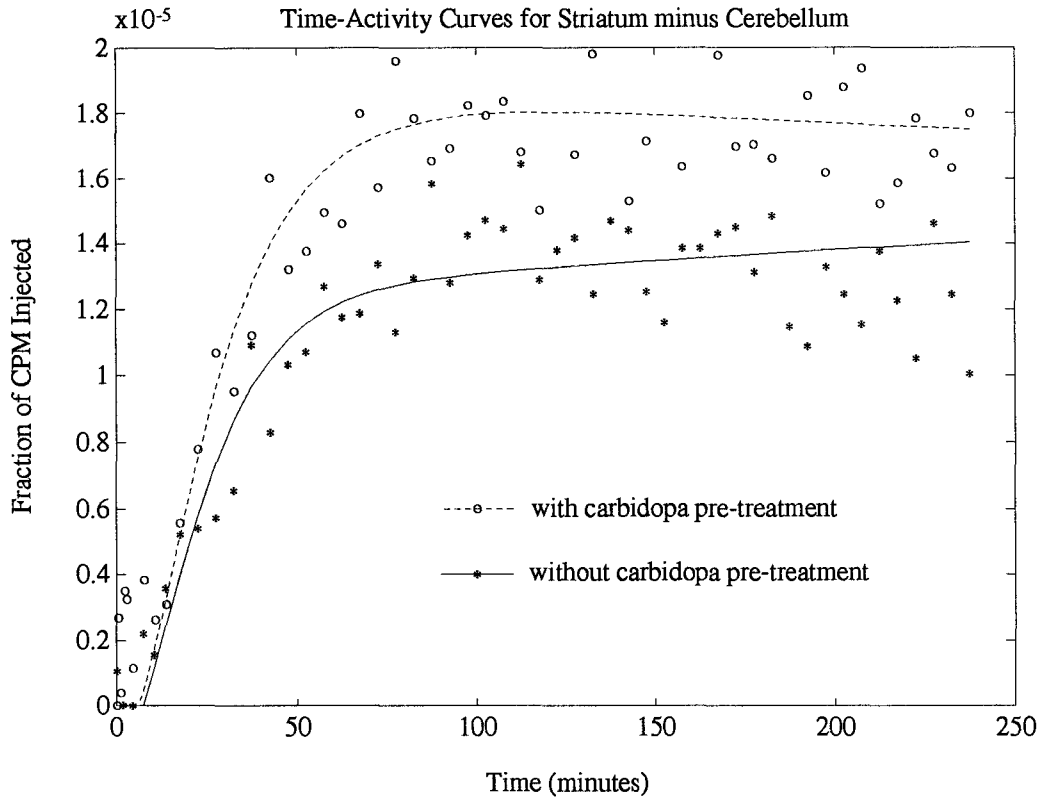

Figure 16: Radioactivity in the striatum minus radioactivity in the cerebellum, plotted against time, with and without carbidopa pre-treatment.

Sensitivity Analyses

The results of the graphical and compartmental analyses are influenced by various factors, such and the shape of the input function or the noise contribution in the PET data. In order to determine the sensitivity of the parameters to these factors, various sensitivity analyses have been performed.

The standard deviation of each parameter, for the cerebellar and striatal models, was estimated from the covariance matrix (Landaw and diStephano, 1984). This standard deviation measures the precision with which the variables can be determined for a given dataset. The standard deviation of K_1 and k_2 in the cerebellum are 0.85% and 0.93% respectively; both of these parameters are thus well-determined by the analysis. The standard deviations for the striatal model are 1.13%, 1.36%, and 4.66%, for K_1, k_2 and k_3 respectively, indicating that the model is less able to determine k_3. The analysis of patients with Parkinson's disease and patients taking neuroleptic medication, however, has shown that values for k_3 may differ by a factor of 2 or more, both above and below normal values. In light of this wide range of measured variation, the variation attributable to the optimization procedure is small. This analysis indicates that measured differences of 10 or 15 percent in k_3 are insignificant.

Sensitivity to the Data Measured by the Tomograph

Effects of Random Noise --

A cylindrical phantom (10 cm radius) containing a solution of ^{68}Ge was used to study the impact of counting statistics on the data measured by the tomograph. ^{68}Ge ($T_{1/2}$ = 270 days) decays by negative β decay to ^{68}Ga ($T_{1/2}$ = 68 min). This isotope decays by positron emission and exists in secular equilibrium with ^{68}Ge so that the decay of the source is negligible over the course of the measurement. One hundred

images ("frames") at 5 minutes per image were acquired, for a total of over 350 million events in the entire study. Circular regions of interest, centered in the field of view, were drawn with radii that ranged from 1.9 to 91.3 mm. The standard deviation of the pixel values in the region was calculated for each region in each frame, and averaged over the 100 frames. This is a measure of the ability of the imaging system to approximate the uniform distribution, and will be referred to as the *spatial* standard deviation of the measured data. The average counts per pixel was also calculated for each region in each frame, and the standard deviation of this value, across the 100 frames, was determined. This value reflects the variance in the mean counts in a region when measured many times, and will be referred to as the *temporal* standard deviation of the measured data. In a system with constant spatial standard deviation, larger regions give more precise estimates of the mean counts per pixel in the region, and will therefore have smaller temporal standard deviations.

The results of this analysis appear in Table 7. The spatial standard deviation, averaged over 8 regions, is 36.0 percent (the three smallest regions have been omitted from this calculation). The temporal standard deviation decreased with increasing region size. The average total counts in each region, and the reciprocal of the square root of this value, are also provided in the table for comparison; the latter measure is the standard deviation of the mean counts in the region, under the assumptions of Poisson counting statistics (Enge, 1966). Note the close agreement between the predicted (counting) and measured (temporal) standard deviations.

TABLE 7

SPATIAL, TEMPORAL AND THEORETICAL STANDARD DEVIATIONS FOR CIRCULAR REGIONS OF INTEREST OF VARYING RADII IN A UNIFORMLY DISTRIBUTED SOURCE OF RADIOACTIVITY.

Radius (mm)	Number of pixels	Total Counts	σ_s* (%)	σ_t† (%)	σ_p‡ (%)
1.9	4	5	21.07	28.80	42.85
3.9	17	23	27.81	22.74	20.89
5.8	21	28	29.14	21.24	18.83
7.8	41	52	34.75	15.68	13.83
9.7	67	86	35.39	11.88	10.78
13.6	133	167	37.46	7.95	7.74
15.5	198	250	37.30	6.11	6.32
19.4	308	395	36.58	4.44	5.03
29.1	698	896	36.16	2.56	3.34
40.8	1378	1762	35.41	1.93	2.38
91.3	6918	8206	34.74	0.74	1.10

*σ_s refers to the spatial standard deviation, as described in the text.
†σ_t refers to the temporal standard deviation, as described in the text.
‡σ_p refers to the theoretical (counting) standard deviation, as described in the text.

For a region of interest defined around the striatum, typical pixel values range between 0.0042 and 0.0055 counts per second per pixel, for a mid-study (300 second) frame. For an average region of interest of 250 pixels in the striatum, this yields between 315 and 412 total counts in the region. The theoretical temporal standard deviation is then 4.92 to 5.63 percent. Using Table 7, an empirical estimate of this value can also be made: since the 19.4 mm region contains 395 total counts, the temporal standard deviation should be greater than or equal to 4.44 percent. Thus, by

both empirical measures and theoretical predictions, 5 percent is a reasonable estimate of the random noise contribution to the measured data.

A simulation approach was used to estimate the variation in the parameters due to this random noise in the data measured by the tomograph. This method yields a measure of the expected variation if measurements of precisely the same physiological situation could be repeated many times. First, a set of parameters were chosen to represent this physiological "truth". The continuous time-activity curve determined by these parameters was then calculated and sampled at the discrete times determined in the F-dopa/PET scanning protocol. This corresponds to a noiseless measurement of the system. A "noisy" time-activity curve was then generated by adding random noise contributions to each time point in the curve. The noise was sampled from a Gaussian distribution with mean 0 and a standard deviation of 5%. Fifty such "noisy" curves were generated (see Figure 17), and analyzed by both compartmental and graphical methods, to produce fifty estimates of each parameter.

The mean, standard deviation and percent standard deviation, as determined by this method, for each of the compartmental and graphical parameters are given in Table 8. In the cerebellum, the distribution volume is seen to be much less sensitive to noise than the rate constants; the graphically determined distribution volume ($V_{e,g}$) is slightly less sensitive than the calculated value ($V_{e,c} = K_1/k_2$). In the striatum, k_3, $K_{i,c}$ and $K_{i,g}$ are about equally sensitive to measurement noise; in this case the calculated influx

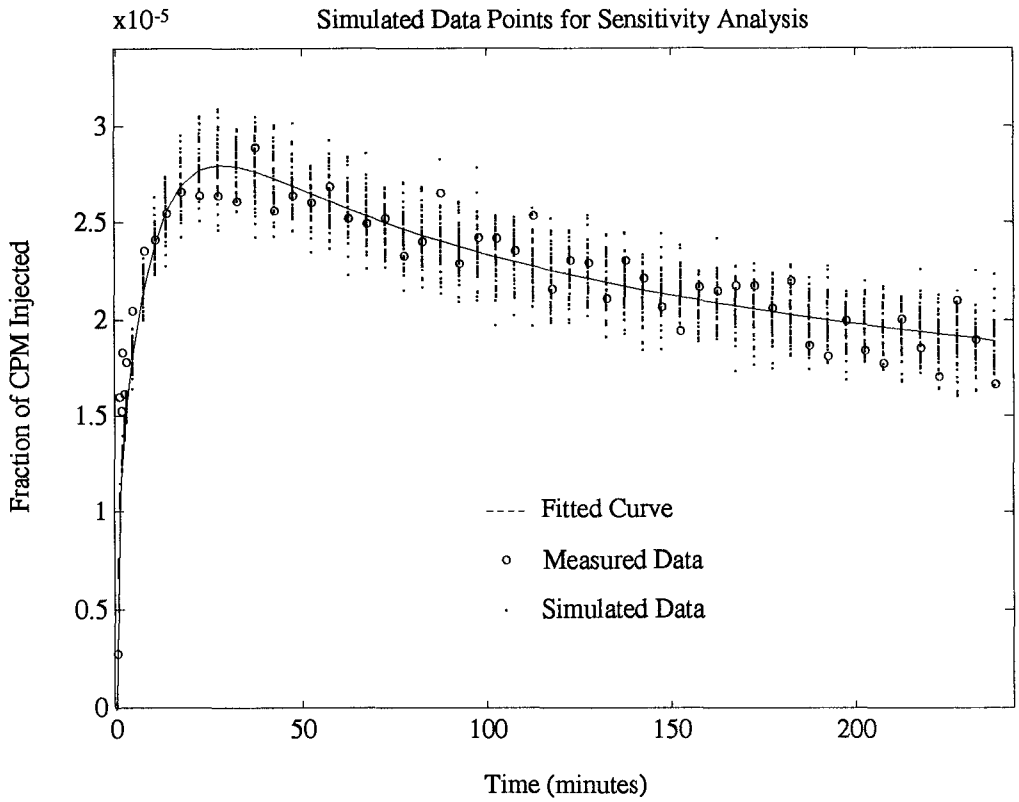

Figure 17: Simulated data points for analysis of the effects of random noise. The original measured points and fitted curve are shown, along with the fifty simulated measured points at each time point.

constant is slightly less sensitive than the other measures. Since these standard deviations reflect the expected variation in the results when the same physical situation is measured, it is clear that differences in parameter estimates of 8 or 10 percent are not significant.

TABLE 8

VARIATION IN THE SOLUTION PARAMETERS OF COMPARTMENTAL AND GRAPHICAL ANALYSES, FOR REPEATED MEASUREMENTS OF THE SAME SYSTEM.

3		K_1 (ml/min/ml)	k_2 (min^{-1})	$V_{e,c}$ (ml/ml)	$V_{e,g}$ (ml/ml)
cerebellum:	mean	0.0393	0.0613	0.6406	0.6407
	SD	0.0018	0.0027	0.0042	0.0034
	%SD*	4.61	4.40	0.65	0.53
	%SD(cov)†	0.85	0.93		

		K_1 (ml/min/ml)	k_2 (min^{-1})	k_3 (min^{-1})	$K_{i,c}$ (min^{-1})	$K_{i,g}$ (min^{-1})
striatum:	mean	0.0341	0.0286	0.0028	0.0030	0.0029
	SD	0.0010	0.0012	0.0001	0.0001	0.0001
	%SD*	2.92	4.04	4.23	3.06	4.15
	%SD(cov)†	1.13	1.36	4.66		

%SD is the standard deviation expressed as percent of the mean, equal to 100(SD/mean).
†%SD(cov) is the standard deviation determined from the covariance matrix, provided for comparison.

Effects of Region of Interest Selection --

To determine the sensitivity of the results to the region of interest selected in the image, 5 different individuals independently outlined the left and right striatum and the cerebellum for a particular study. The resulting time-activity curves were analyzed; the compartmental and graphical parameters are tabulated in Table 9, along with the

mean and standard deviation of each parameter. The number of pixels in each region is also provided in the table.

Several conclusions may be drawn from this analysis. The variations in K_1, k_2, $K_{i,c}$ and $K_{i,g}$ due to changes in the region of interest, for both the cerebellum and

TABLE 9

EFFECTS OF REGION OF INTEREST SELECTION ON COMPARTMENTAL AND GRAPHICAL PARAMETERS, FOR THE STRIATUM AND CEREBELLUM.

	ROI Number	ROI area (pixels)	K_1 (ml/min/ml)	k_2 (min^{-1})	$V_{e,c}$ (ml/ml)	$V_{e,g}$ (ml/ml)
cerebellum:	1	781	0.0390	0.0548	0.712	0.713
	2	434	0.0424	0.0570	0.744	0.741
	3	1279	0.0360	0.0536	0.671	0.675
	4	659	0.0412	0.0570	0.721	0.725
	5	729	0.0399	0.0560	0.712	0.715
	mean	776	0.0397	0.0557	0.7124	0.7146
	SD	310	0.0024	0.0015	0.0262	0.0252
	%SD	40	6.16	2.70	3.67	3.53

	ROI Number	ROI area (pixels)	K_1 (ml/min/ml)	k_2 (min^{-1})	k_3 (min^{-1})	$K_{i,c}$ (min^{-1})	$K_{i,g}$ (min^{-1})
striatum:	1	288	0.0331	0.0280	0.0027	0.0030	0.0027
	2	146	0.0380	0.0335	0.0028	0.0029	0.0026
	3	363	0.0364	0.0363	0.0027	0.0025	0.0021
	4	301	0.0364	0.0347	0.0027	0.0026	0.0023
	5	160	0.0355	0.0306	0.0028	0.0030	0.0027
	mean	251	0.0359	0.0326	0.0027	0.0028	0.0025
	SD	94	0.0018	0.0033	0.0001	0.0002	0.0002
	%SD	37	4.98	10.2	2.03	8.22	9.84

striatum, are greater than (but of the same order of magnitude as) the variations expected as a result of random noise. This indicates that these parameters are somewhat sensitive to region of interest selection. The 2% standard deviation of k_3, however, indicates that this parameter is relatively insensitive to the region chosen. It is worth noting at this point that the sizes of the five regions chosen vary by a factor of two and three in the striatum and cerebellum respectively. This emphasizes the inherent subjectivity in user-defined borders. In light of these vast differences in border definition, the relatively small variation in the parameters demonstrates the stability of the analysis. Nevertheless, a more objective means of region of interest selection should be implemented.

Sensitivity to the Plasma Curve

Effect of Timing Errors --

During the course of a two hour study, plasma samples are taken according to the protocol previously outlined. As the samples are taken, the exact time is read from a stop-watch and recorded by hand. To investigate the sensitivity of the analyses to random errors in this timing, a simulation technique was used. First, a set of three exponentials were chosen as representative of a typical blood curve. A continuous time-activity curve was calculated from these parameters, and sampled at the discrete times determined by the sampling protocol. This corresponds to a blood curve sampled

with no timing errors. A random timing error was then added to each point in the curve; this error was sampled for each time point from a Gaussian distribution with mean 0 and a standard deviation of 2 seconds, a generous estimate. Fifty simulated plasma time-activity curves were produced in this way, and used as the input function in compartmental and graphical analyses of the striatum. The same measured striatal activity curve was used in each of the fifty simulations.

The effect of delay in the plasma time-activity curve was investigated in a similar manner. The time at which the bolus reaches the brain is approximated by examining PET images of the posterior part of the venous sinus. These images are acquired at a rate of 6 per minute for the first 2 minutes of the scan. If the peak time for the blood is set at the middle of the peak frame for the venous sinus, a positive or negative 5 second timing error is still possible. To determine the effect of these errors, the same random delay, sampled from a uniform distribution ([-5,5] seconds), was added to every point in a noise-free plasma curve; 50 simulated plasma time-activity curves were analyzed by compartmental and graphical analyses.

TABLE 10

EFFECTS OF RANDOM TIMING ERRORS AND DELAY IN THE MEASURED TIME-COURSE OF RADIOACTIVITY IN PLASMA: VARIATION IN COMPARTMENTAL AND GRAPHICAL PARAMETERS FOR THE STRIATUM*.

	K_1	k_2	k_3	$K_{i,c}$	$K_{i,g}$
Timing	3.10	3.99	4.47	3.53	0.08
Delay	1.87	1.09	4.33	2.80	0.21

values are given as percent standard deviation, equal to 100(SD/mean)

The standard deviations determined by these methods, for timing and delay errors, are given in Table 10. The errors for each parameter are approximately equal to or less than the standard deviations of the parameters due to random noise. It was therefore concluded that the results of both analyses are insensitive to these errors.

Effect of the Peak Shape --

When arterialized venous blood is sampled as an estimate of the arterial feed to the brain, the measured peak, or bolus, is dispersed (Zierler, 1965). In this analysis, the peak height was set at the ratio of the dose injected to the plasma volume; this assumes instantaneous mixing throughout the plasma. While complete mixing does not likely occur before the intravenously injected bolus reaches the brain, this correction offers a consistent means of determining the peak height in different individuals. A plasma volume estimate of 35 ml/kg has been used in this analysis; this value is typically estimated at 35 to 40 ml/kg.

To investigate the effects of changes to the peak height on the parameter estimates, three simulated blood curves were created with peak heights equal to 1.15, 1.5 and 2 times the peak calculated from the plasma volume. The 15% increase corresponds to a plasma volume estimate of 40 ml/kg. The 200% increase corresponds to the bolus mixing through half the plasma volume before reaching the brain. Compartmental and graphical analyses were performed using each of these curves.

Increases in the peak width were investigated by the same method, and the results of both investigations appear in Table 11. From these data the following conclusions can be drawn: none of the parameters are sensitive to a 15% change in the peak height; the graphically determined influx constant is much less sensitive to changes in the shape of the peak than $K_{i,c}$; k_3 is most sensitive to changes in peak width, but all of the compartmental parameters show sensitivity to the height and width of the peak.

These results indicate that the early shape of the blood curve, particularly the peak width, has a significant effect on the results of the compartmental analysis. Accurate characterization of the early points of this curve is therefore crucial.

TABLE 11

EFFECTS OF CHANGES IN PEAK HEIGHT AND PEAK WIDTH OF INPUT FUNCTION: PERCENT CHANGE* IN COMPARTMENTAL AND GRAPHICAL PARAMETERS FOR STRIATUM.

	K_1	k_2	k_3	$K_{i,c}$	$K_{i,g}$
peak+15%	1.7963	1.7498	0.4012	0.5752	0.8176
peak+50%	9.9054	10.7182	7.3178	6.8041	2.6744
peak+100%	20.5839	20.5686	15.6590	16.1571	5.2095
width+15%	3.4642	7.6688	19.8434	15.1529	0.3082
width+50%	6.9063	10.7293	20.5320	16.2739	1.0973
width+100%	9.6591	13.0777	20.0210	16.2534	2.4775

*values provided are absolute percent change, equal to $|100*(k_{new} - k_{old})/k_{old}|$

Summary

A simple graphical method and a simple compartmental model have been proposed, in order to study the time-course of radioactivity in the striatum after an F-dopa injection. Both methods are mathematically justifiable, and the results of each can be compared, providing an internal standard. The methods have been tested in fourteen F-dopa/PET studies, and the influx constants derived by each analysis are in excellent agreement. Both analyses respond to perturbations in the physiology, as suggested by the results obtained for Parkinsonian patients, and for patients taking neuroleptic medication. A summary of these results appears in Table 12; the values

TABLE 12

COMPARISON OF COMPARTMENTAL AND GRAPHICAL RESULTS FOR NORMAL CONTROLS, PATIENTS WITH PARKINSON'S DISEASE AND PATIENTS ON NEUROLEPTIC MEDICATION*.

Study Numbers	k_3 (min^{-1})	$K_{i,c}$ (min^{-1})	$K_{i,g}$ (min^{-1})
1 and 2 (controls)	0.0043	0.0037	0.0037
9 and 10 (Parkinsonian)	0.0012	0.0011	0.0010
5 and 6 (Neuroleptic)	0.0098	0.0055	0.0055

* In each case, the average parameter for two studies in different individuals is given; values for the putamen on the more afflicted side of the Parkinsonian patients were used.

calculated for k_3, $K_{i,c}$, and $K_{i,g}$ are lower than normal for Parkinsonian patients, and higher than normal for patients taking neuroleptics.

The graphically determined influx constant is less sensitive to distortions in the shape of the arterial blood time-activity curve, and is therefore a valuable measure for inter-subject and inter-group comparison. Because a wide variation in this parameter is possible when computed on the basis of a two hour study, graphical results should be verified by completing the compartmental analysis and computing $K_{i,c}$. The rate constants of the compartmental model may provide additional information for specific individuals.

It has also been concluded that the advantages of pre-treatment with carbidopa are negligible, and that accurate characterization of the time-course of radioactivity in the plasma is crucial.

Chapter 5

Discussion

It is clear that the compartmental and graphical methods proposed, conducted in parallel with each other, offer an informative and methodologically sound analysis of positron tomographic studies which use F-dopa as a tracer for intracerebral dopamine metabolism in man. The ability of both methods to reflect physiological perturbations has been clearly demonstrated, and the sensitivity of each method to random errors in the measurement of radioactivity in both the brain and the blood has been critically examined.

It has been demonstrated that the graphical method used is a valid application of the original derivation by Patlak et al. (1983), and that the conditions of the Patlak model have been met. Some of the more basic assumptions underlying compartmental analysis, however, have remained unanswered.

The Assumptions Re-examined

The first question is that of stationarity: is the impulse response of the model constant at all points during the experiment? Since the impulse response in this case

corresponds to a variety of metabolic and transport processes in a living human being, this assumption is clearly invalid. While small fluctuations in these processes will be masked by the five minute integration of the positron tomographic frame, many of the time-activity curves in the brain seem to exhibit low amplitude oscillations with frequencies of thirty to sixty minutes (see Figure 18). These oscillations cannot be predicted by the simple model proposed, and may result from the dynamic nature of the impulse response for this system. The larger pattern of the kinetics of the radiolabel in the brain, however, is not obscured by these fluctuations, and it is this pattern that is currently of clinical interest. In short, the system is not stationary, but it is stationary enough for the purpose of these investigations.

The second question is that of linearity: does the flux from one compartment to the next depend only upon a rate constant and the concentration in the first compartment? Once again, this assumption in likely wrong. Neff reports that AADC activity is modulated by neurotransmitter receptors, and it has long been established that tyrosine hydroxylase activity is moderated by the concentration of dopamine in the striatum. Thus, if any of the rate constants reflect AADC activity, the concentration of the *product* molecule may effect the rate of flux. Since only tracer quantities are injected and monitored, however, the changes in total striatal concentrations effected by the filling or emptying of the various compartments become negligible. Once again, the system is linear enough for the present purpose.

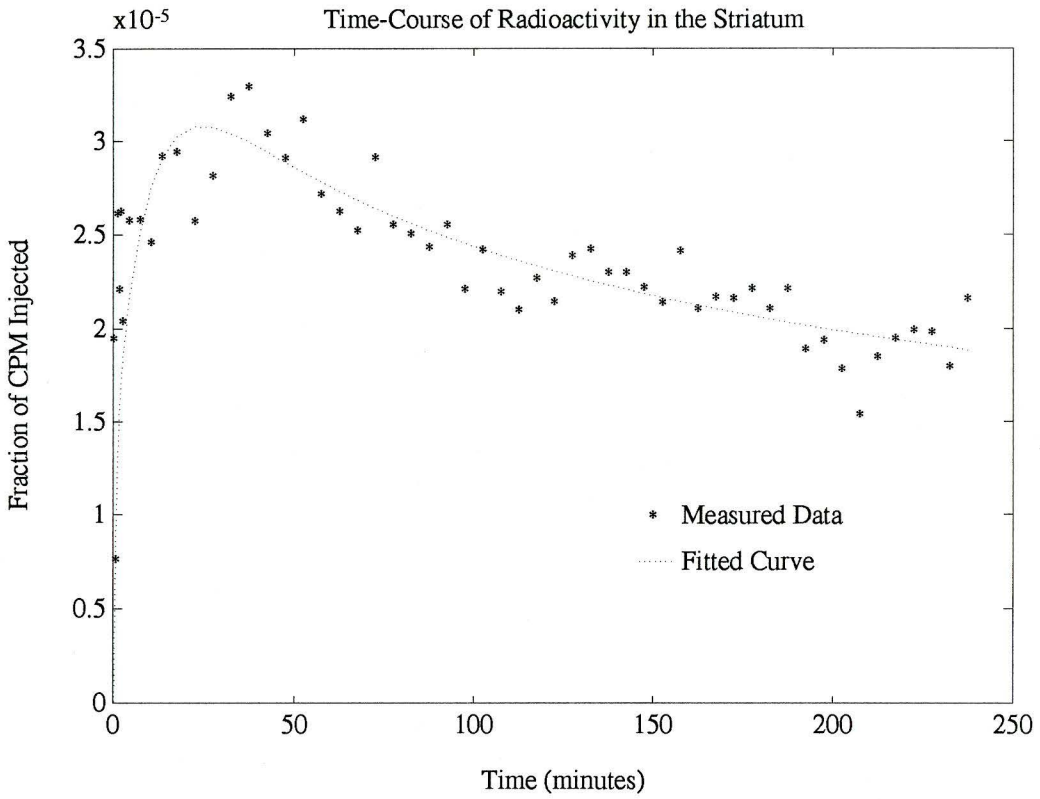

Figure 18: Time-course of radioactivity in the striatum, after an F-dopa injection. Note the apparent pattern of oscillations, particularly between 100 and 200 minutes.

This discussion of the assumptions, however, touches upon another fundamental issue which has not yet been addressed: no attempt has been made to assign any physical meaning to the compartments or rate constants. Although this might suggest that the entire procedure has been "an exercise in curve-fitting" (Zierler, 1981, p. 544), some compelling arguments about the physiology of the system can be made. These deductions must be made cautiously, however, to ensure that the model is not "over-interpreted" -- that is, to ensure that meaning is not assigned for the sake of assigning meaning, in the absence of clear evidence.

Consider the two-compartment model proposed for the striatum. The components of this model -- the compartments, the input function and the three rate constants -- will first be examined in general, and a physical interpretation of the input function will be given. The physical meaning of the second compartment will then be discussed. The first compartment can then be understood in relation to the input function and the second compartment. This understanding, in turn, will allow for a strict definition of the rate constants.

It is clear that the two compartments correspond to the presence of the radiolabel in the brain, specifically in striatal tissue. Although this "tissue" would be ideally composed of the endings of dopaminergic neurons alone, other neurones and glial cells are present in the region. The heterogeneity of striatal tissue at the cellular level matters little to the analysis, however, since averages are taken across regions of the order of cubic centimeters. The input function corresponds to the presence of the radiolabel in the plasma, in the form of F-dopa and its metabolites; this function feeds the first compartment. K_1 must then reflect the transport of the label out of the blood and into the first compartment; k_2 must represent the reverse process.

It has been shown that, of the metabolites of F-dopa, only OMFD enters the brain (Garnett and Nahmias, personal communication). K_1 then represents the transport of F-dopa *and* OMFD out of the blood and into the first compartment, which must

include both of these labelled molecules. Because of the presence of both K_1 and k_2, the first compartment, by definition, equilibrates with the plasma. This implies that the first physical or metabolic step taken by labelled molecules which prevents equilibrium, that is, the first step into an *irreversible* compartment, must be assigned to k_3. This is neither mathematical wizardry nor clever rhetoric; it is a feature of the model, by definition. The first physiological process which effects either F-dopa or OMFD (or both), such that they can no longer equilibrate with labelled molecules in the plasma, can and must be assigned to k_3.

Studies after the injection of OMFD have illustrated that this molecule comes into equilibrium with the plasma throughout the brain. OMFD, therefore, is confined to the first compartment. What process in the transport or metabolism of F-dopa, then, corresponds to the irreversible rate constant, k_3?

It has been shown that the distribution of radioactivity in the striatum is correlated with blood flow for the first five minutes after injection, and thereafter correlated to endogenous catecholamine content (Horne et al., 1984), that the half life of striatal fluorodopamine is at least sixty minutes (Firnau et al., 1987; Barrio et al., 1990), and that the efflux of DOPAC and HVA (the metabolites of dopamine) is slow (Firnau et al., 1984). It has also been suggested that fluorodopamine in the striatum is associated with the vesicles (Diffley et al., 1983), and the striatal retention of ^{18}F activity is reported to be reduced by the administration of inhibitors of vesicular storage

(Pate et al., 1990). In summary, there is substantial evidence to indicate that fluorodopamine formed in the neurons is not in equilibrium with labelled molecules in the blood. The *decarboxylation* of F-dopa in striatal neurons, which prevents F-dopa in the striatum from reaching equilibrium with plasma concentrations, must therefore be assigned to k_3.

Since k_3 represents the decarboxylation of F-dopa, the second compartment must represent the presence of fluorodopamine and its labelled metabolites (predominantly DOPAC and HVA) in striatal tissue. There is evidence to suggest that much of the fluorodopamine in this compartment is associated with striatal vesicles, however this is immaterial to the analysis.

Having thus defined the input function and the second compartment, the physical meaning of the first compartment is directly derivable. Simply put, the first compartment corresponds to the presence of labelled molecules in striatal tissue which have left the blood and have not been decarboxylated within the neurons. This compartment will contain OMFD and F-dopa in striatal tissue, and may also include labelled molecules within the walls of the capillary endothelium, interposed between blood and brain. In a study of the blood-brain barrier, Bertler et al. (1966) demonstrated the presence of both monoamine oxidase and AADC in the capillary endothelial cells. Wade and Katzman (1975) observed fluorescence (due to L-dopa and dopamine) in the capillary endothelium of rats' brains after an injection of L-dopa. It

can be therefore concluded that the capillary endothelial cells have the capacity to retard and regulate the influx of F-dopa to the striatum. This known physiology, however, does not alter the fact that the data will only support a two-compartment, three-parameter model, nor does it bear upon the arguments provided for the physical meaning of the second compartment. Since dopamine formed within the capillary walls has been found to disappear rapidly (Bertler et al., 1966), this decarboxylation does not represent an irreversible trapping of the tracer. The presence of labelled molecules within the cells of the capillary walls must therefore be included in the first compartment, which contains every transport or metabolic process undergone by labelled molecules after leaving the blood, except those which occur after the decarboxylation of F-dopa within the neurons.

With the compartments defined in this way, K_1 and k_2 must measure the forward and reverse transport rates of the labelled molecules out of and into the plasma, while k_3 is a measure of AADC activity within the neurons. Since AADC activity is correlated with tyrosine hydroxylase activity, k_3 is a measure of endogenous dopamine formation. This would agree with the findings that k_3 in Parkinsonian patients is low; the loss of nigrostriatal neurons has effected a net decrease in dopamine synthesis in this area. In patients taking neuroleptic medication, the increased firing rate of nigrostriatal neurons may cause an accelerated synthesis of dopamine (Seeman, 1989); this is in agreement with the findings that k_3 is high for these patients. Finally, k_3 has been found to be negligible for a non-dopaminergic

region of the brain, and after OMFD injection. These results each independently verify the physical meaning assigned to the compartments and rate constants of the model.

It also clear from these considerations that in the cerebellum, a non-dopaminergic region of the brain, the single compartment represents the presence of F-dopa and OMFD in cerebellar tissue. The rate constants K_1 and k_2 then measure the forward and reverse transport rates out of and into the plasma in this region.

The influx constant for this system is highly correlated with measured k_3 values. Nevertheless, K_i does incorporate contributions of the other rate constants of the model (see Equation 17), which represent the rates of transport of L-dopa and OMFD across the blood-brain barrier. It is thus inarguably valuable to conduct the compartmental and graphical analyses independently, and to use the results of each to serve different clinical and research purposes.

Suggestions for Further Work

The ability of these analyses to reveal and quantify differences in the dopaminergic metabolism of individuals has been demonstrated in a small number of studies. Further clinical studies should be undertaken in order to investigate the response of the model to physiological perturbations and thus justify the physical meaning attributed to the various compartments and rate constants.

Although the clinical value of these analyses has been demonstrated, the major limitation of both methods is that OMFD is included in the reversible region. In both the graphical and compartmental analysis, this inclusion is mathematically valid. In order to compare results between subjects, however, the assumption must be made that the proportion of OMFD in the plasma is the same for different individuals. Recent studies have reported a large inter-subject variability in peripheral O-methylation rates (Huang et al., 1991). While it is unlikely that the data will stand a correction for this effect (as evidenced by the fact that a two-compartment model gives the statistically best fit to the data), the exact influence of the O-methylation rate should be further studied.

To determine the effects of different O-methylation rates in the periphery, simulation studies could be run, in which "true" rate constants for blood-brain barrier transport of OMFD and F-dopa, and for AADC activity are separately hypothesized. These could be used to calculate the impulse responses for both OMFD and F-dopa in the brain, assuming there is negligible O-methylation within striatal tissue. A single blood curve could then be decomposed into a hypothetical sum of OMFD and F-dopa contributions; these separate curves could be used as inputs to the parallel models, and the resulting time-activity curves summed. This would produce a predicted time-activity curve, which could be solved by compartmental and graphical analyses. The results of these analyses could then be compared for different ratios of OMFD and F-

dopa in the blood. In this procedure, the physiology is fixed by the "true" rate constants, and differences in the calculated parameters are attributable only to different peripheral O-methylation rates.

Another suggestion for further research is the independent measurement of the range of normal O-methylation rates in humans. Further F-dopa studies should therefore be performed, and the blood samples should be analyzed for the contribution of the metabolites, especially OMFD. In this way, a range of values for study by the simulation analysis above can be established.

Finally, the results of these further F-dopa studies, in which the time course of OMFD and F-dopa in the blood have been determined, might be used to determine whether a correction for OMFD in the brain should be made. The simplest compartmental model which includes the contribution of OMFD, that is, the addition of a reversible compartment in parallel with the first compartment of the striatal model, may be analyzed using the separate time courses of OMFD and F-dopa in the blood in parallel. The results of this analysis, which will include two additional parameters and some error in the blood decomposition, can be compared to results obtained for the same studies in the simpler model. The standard deviation of the rate constant which represents AADC activity in each case should be compared. In this way, the model which best determines this parameter, in a statistical sense, can be identified.

Appendix

This appendix lists the code for the following routines, written for the MATLAB programming environment (The MathWorks, Inc., 1990):

Compartmental Analysis Routines

Graphical Analysis Routines

Sensitivity Analysis Routines

```
%%%%%%%%%%%%%%%%%%%%%%%%%%%%%%%%%%%%%%%%%%%%%%%%
%
%  solve.m -- Compartmental Analysis Routine
%
%             Given an initial set of parameters, this routine computes
%            the impulse response of a given model, and convolves it with
%             the given input function.  The result is compared to the
%            given output and the parameters altered until the predicted
%             and measured output match most closely.
%
%  requires:
%     pet[n,2] -- column of times and column of measured data from PT
%     blood[m,2] -- column of times and column of measured data from blood
%     param[p] -- row of initial estimates for parameters
%     model -- three character string, see "make_coef.m"
%     tolerance -- precision required, usually between 0.01 and 0.0001
%
%  produces:
%     brain_est[n] -- column of points for best fit, at times in "pet"
%     param[p] -- solution parameters
%     chisquare,per_diff -- measures of goodness of fit
%     y -- weighted least sum of squares, for F-test
%     ki,int -- slope and intercept of patlak plot, calculated from param
%     kil,intl -- slope and intercept of logan plot, calculated from param
%
%%%%%%%%%%%%%%%%%%%%%%%%%%%%%%%%%%%%%%%%%%%%%%%%
global NCOMP       %  number of compartments %
global model       %  string describing model %
global pet         %  measured data from tomograph %
global blood_lin   %  blood curve, at equal time points %
global brain_est   %  estimated fit to pet data %
global times       %  times at which fit is computed and compared %
global step_size   %  space between each point in "times" %
global coef        %  coefficients of differential equations of model %
global cparam      %  constrained parameter -- value does not change %
global k_one       %  parameter by which blood curve is multiplied, K1 %
%
clear x0 x xdot       %  must be cleared for multiple runs %
output = 1;        %  output = 0 --> no output to screen from optimization
%
%
%  setup times for blood and pet data at equal intervals %
step_size = pet(2,1) - pet(1,1);
times = [ pet(1,1):step_size:pet(length(pet),1) ];
ltim = length(times);
  if times(ltim) < pet(length(pet),1)
    times = [ times times(ltim)+step_size ];
    ltim = ltim+1;
  end
bltimes = [];
for i = 1:ltim
  if times(i) < blood(length(blood),1)
    bltimes = [ bltimes times(i) ];
  end
end
%  evaluate blood curve at equal time intervals  %
blood_lin = table1(blood,bltimes);
```

```
%  correct convolution if the first time is zero %
if bltimes(1) == 0
  blood_lin(1) = blood_lin(1)/2;
end
%  optimize the function "cost.m"  %
min = fmins('cost',param,tolerance,output);
%  save the old parameters, set param to the optimized values %
oldparam = param;
param = min;
%  plot the results %
plot(pet(:,1),brain_est,pet(:,1),pet(:,2),'*')
qtitle
%  calculate the graphical plots and intercepts %
[ki,int]  = make_ki(min);
[kil,intl] = make_logan(min);
%  evaluate measures of goodness of fit %
chi2 = chisquare(pet(:,2),brain_est)
per_diff = pdiff(pet(:,1),pet(:,2),brain_est)
meas = pet; fit = brain_est;
y = wlss(meas,fit)
```

```
%%%%%%%%%%%%%%%%%%%%%%%%%%%%%%%%%%%%%%%%%%%%%%%%
%
%  cost.m -- calculate the cost function for the current params
%
%%%%%%%%%%%%%%%%%%%%%%%%%%%%%%%%%%%%%%%%%%%%%%%%
function y = cost(param)
%  calculate the fitted curve for the current params %
brain_est = brainint(param);
%  Evaluate squared difference,                                          %
%       weighted by time interval and 1/measured value.                   %
%  For ignoring initial points, set cost_1 to first point to evaluate. %
cost_1 = 1;
petend = length(pet);
y = 0;
 if cost_1 < 2
    y = (pet(1,2) - ...
             brain_est(1))^2*(pet(2,1)-pet(1,1))*(1/pet(1,2));
 end
 for i = cost_1:(petend - 1)
     y = y + (pet(i,2) - brain_est(i))^2...
              *(pet(i+1,1) - pet(i-1,1))*(1/pet(i,2));
 end
y = y + (pet(petend,2) - brain_est(petend))^2...
         *(pet(petend,1) - pet( petend - 1,1))*(1/pet(petend,2));
```

```
%%%%%%%%%%%%%%%%%%%%%%%%%%%%%%%%%%%%%%%%%%%%%%%%
%
%  brainint.m -- evaluate the fitted curve for the given params
%
%%%%%%%%%%%%%%%%%%%%%%%%%%%%%%%%%%%%%%%%%%%%%%%%
function brain_est = brainint(param)
%  make the coefficient matrix for the differential equations  %
coef = make_coef(param);
%  set the initial conditions for an impulse response  %
x0(1) = 1;
for icomp = 2:NCOMP
  x0(icomp) = 0;
end
%  integrate the diffyq with these initial conditions  %
[t,x] = ode45('diffyq',0,times(length(times)),x0);
%  sum the results for each compartment  %
xsum = x(:,1);
for icomp = 2:NCOMP
  xsum = xsum + x(:,icomp);
end
%  evaluate the summed response at "times"  %
tab = [t xsum];
xsum_lin = table1(tab,times);
if times(1) == 0
  xsum_lin(1) = xsum_lin(1)/2;
end
%  perform the convolution with the blood, multiply by K1 and step_size
%
brain_est = conv(xsum_lin,blood_lin);
brain_est = brain_est*k_one*step_size;
%  evaluate the results of the convolution at the times given in "pet"
%
long_times = [ 0:length(brain_est)-1 ];
tab2 = [ times(1)+(long_times*step_size)' brain_est];
brain_est = table1(tab2,pet(:,1));
```

```
%%%%%%%%%%%%%%%%%%%%%%%%%%%%%%%%%%%%%%%%%%%%%%%%
%
%  make_coef.m -- setup the coefficients for the differential equations
%       Each model is denoted by a 3 character string.
%       The rate of change in the amount of material in comp't i, q_i(t)
%       is given by the sum over j of coef[i,j]*q_j(t).
%
%%%%%%%%%%%%%%%%%%%%%%%%%%%%%%%%%%%%%%%%%%%%%%%%
function coef = make_coef(param)
p = param;
k_one = p(1);

% cerebellum, 1 compt, 1k %
if model == 'cer'
  NCOMP = 1;
  k_one = p(1);
  coef = [ -p(2) ];
end

% cerebellum, 2 compt, 4k %
if model == 'cr4'
  NCOMP = 2;
  k_one = p(1);
  coef = [ -p(2)-p(3)      p(4)
             p(3)          -p(4) ];
end

% striatum, 2 compt, 3k %
if model == 'str'
  NCOMP = 2;
  k_one = p(1);
  coef = [ -p(2)-p(3)    0.0
              p(3)      0.0  ];
end

% striatum, 2 compt, 4k %
if model == 'st4'
  NCOMP = 2;
  k_one = p(1);
  coef = [ -p(2)-p(3)       0.0
             p(3)           -p(4)   ];
end

% striatum, 3 compt, 5k %
if model == 'st5'
  NCOMP = 3;
  k_one = p(1);
  coef = [-p(2)-p(3)  p(4)           0.0
           p(3)       -p(4)-p(5)     0.0
           0.0         p(5)          0.0 ];
end
```

```
% blood, 3 compt, 6 k %
if model == 'bld'
  NCOMP = 3;
  k_one = cparam;
  coef = [ -p(1)-p(2)-p(4)  0.0                    0.0
             p(2)                      -p(3)           0.0
             p(4)                       0.0            -p(5)   ];
end


% blood, 2 compt, 3k %
if model == 'bl3'
  NCOMP = 2;
  k_one = cparam;
  coef = [ -p(1)-p(2)  0.0
             p(2)       -p(3) ];
end
```

```
%%%%%%%%%%%%%%%%%%%%%%%%%%%%%%%%%%%%%%%%%%%%%%%%
%
%  diffyq.m -- the differential equations
%
%  The notaion x' is interpreted by MATLAB as dx/dt.
%  Note that x and xdot have NCOMP columns.
%
%%%%%%%%%%%%%%%%%%%%%%%%%%%%%%%%%%%%%%%%%%%%%%%%
function xdot = diffyq(t,x)
xdot = zeros(NCOMP,1);
xdot = coef*x';


%%%%%%%%%%%%%%%%%%%%%%%%%%%%%%%%%%%%%%%%%%%%%%%%
%
%  chisquare.m -- evaluate chisquare goodness of fit
%
%%%%%%%%%%%%%%%%%%%%%%%%%%%%%%%%%%%%%%%%%%%%%%%%function    chi2    =
chisquare(y1,y2)
chi2 = 0;
for i = 1:length(y1)
  if y2(i) ~= 0
    chi2 = chi2 + (y1(i) - y2(i))^2/y2(i);
  end
end


%%%%%%%%%%%%%%%%%%%%%%%%%%%%%%%%%%%%%%%%%%%%%%%%
%
%  pdiff.m -- average percent diffence between fitted and measured points
%             weighted by time interval
%
%%%%%%%%%%%%%%%%%%%%%%%%%%%%%%%%%%%%%%%%%%%%%%%%function    pdiff    =
pdiff(x,y,ytrue)
pdiff = 0;
xend = length(x);
w(1) = (x(2)-x(1))/2;
w(xend) = (x(xend) - x(xend-1))/2;
for i = 2:xend-1
  w(i) = (x(i+1) - x(i-1))/2;
end
for i = 1:xend
  if ytrue(i) ~= 0
    pdiff = pdiff + w(i)*abs(y(i) - ytrue(i))/ytrue(i);
  end
end
pdiff = pdiff/(x(xend) - x(1));
```

```
%%%%%%%%%%%%%%%%%%%%%%%%%%%%%%%%%%%%%%%%%%%%%%%%
%
%  wlss.m -- evaluate weighted residual sum of squares
%            weighted by time interval and 1/measured point
%
%%%%%%%%%%%%%%%%%%%%%%%%%%%%%%%%%%%%%%%%%%%%%%%%
function y = wlss(meas,fit)
measend = length(meas);
y = 0;
%
%  for including initial point
%  y = (meas(1,2) - fit(1))^2*(meas(2,1)-meas(1,1))*(1/meas(1,2));
%
 for i = 10:(measend - 1)
     y = y + (meas(i,2) - fit(i))^2...
              *(meas(i+1,1) - meas(i-1,1))*(1/meas(i,2));
 end
y = y + (meas(measend,2) - fit(measend))^2...
         *(meas(measend,1) - meas( measend - 1,1))*(1/meas(measend,2));
```

```
%%%%%%%%%%%%%%%%%%%%%%%%%%%%%%%%%%%%%%%%%%%%%%%%
%
%  make_ki.m -- calculate patlak slope and intercept from params
%
%%%%%%%%%%%%%%%%%%%%%%%%%%%%%%%%%%%%%%%%%%%%%%%%
function [ki,int] = make_ki(param)
%  model == 'st5'  %
if (length(param)) == 5
  K = [-param(2)-param(3)  param(4)
        param(3)          -param(4)-param(5) ];
  Q = [ param(1)
          0     ];
  G = [ 0    0
        0  param(5) ];
  Un = [ 1
         1 ];
end
%  model == 'st3' %
if (length(param)) == 3
  K = [-param(2)-param(3) ];
  Q = [ param(1)];
  G = [ param(3) ];
  Un = [ 1 ];
end
Kbp = 0;
Vp  = 0;
%
ki = -Un'*G*(inv(K))*Q + Kbp
int = -Un'*(K + G)*(inv(K)*inv(K))*Q + Vp
```

```
%%%%%%%%%%%%%%%%%%%%%%%%%%%%%%%%%%%%%%%%%%%%%%%%
%
%  patlak.m -- patlak plot of pet and blood data
%
%  requires:
%     pet[n,2] -- column of times and column of measured pet data
%     blood[n,2] -- column of times and column of measured blood data
%
%  produces:
%     slope -- slope of Patlak plot
%     intercept -- ordinate intercept of Patlak plot
%
%%%%%%%%%%%%%%%%%%%%%%%%%%%%%%%%%%%%%%%%%%%%%%%%
%  setup Am and Cp and AmCptimes from pet and blood data %
prepat
%  evaluate the points to be plotted  %
[xx,yy] = patlak_pts(Am,Cp,AmCptimes);
%  initialize the first set of [x,y] points  %
xshort = xx; yshort = yy;
ktolerance = .01;
deltak = 1.0;
kold = 10;
%  loop until the change in the slope is less than the tolerance  %
for ishort= 2:length(xx)
  % find the best straight line fit through the short set of [x,y] pts %
  k = polyfit(xshort,yshort,1);
  if k(1) ~= 0
    deltak = abs(k(1) - kold)/abs(k(1));
  end
  if deltak < ktolerance, break, end
  kold = k(1);
  %  ignore the first point in the short set and try again %
  xshort = xx(ishort:length(xx));
  yshort = yy(ishort:length(yy));
end
%  print results and plot %
point_1 = length(xx) - length(xshort)
slope = k(1)
intercept = k(2)
fit = polyval(k,xx);
xextrap = xx(1:ishort);
fitextrap = fit(1:ishort);
fitshort = fit(ishort-1:length(xx));
plot(xx,yy,'o',xshort,fitshort,'-',xextrap,fitextrap,'--')
```

```
%%%%%%%%%%%%%%%%%%%%%%%%%%%%%%%%%%%%%%%%%%%%%%%%
%
%  prepat.m -- setup Am, Cp and AmCptimes for pet and blood studies  %
%
%%%%%%%%%%%%%%%%%%%%%%%%%%%%%%%%%%%%%%%%%%%%%%%%
Am = pet(:,2);
AmCptimes = pet(:,1);
Cp = table1(blood,AmCptimes);
%  correct for well-counter calibration if it hasn't been done yet %
if Cp(2)/Am(2) > 1.0e+04
  Cp = Cp*9.381e-8;
end



%%%%%%%%%%%%%%%%%%%%%%%%%%%%%%%%%%%%%%%%%%%%%%%%
%
%  patlak_pts.m -- given Am, Cp, and the times, figure out the points
%                  to plot in a Patlak graphical analysis
%
%%%%%%%%%%%%%%%%%%%%%%%%%%%%%%%%%%%%%%%%%%%%%%%%
function [xx,yy] = patlak_pts(am,cp,t)
cptotal = 0.0;
clear xx yy;
xx(1) = 0;
yy(1) = 0;
if cp(1) ~= 0
  xx(1) = t(1)/2.0;
  yy(1) = am(1)/cp(1);
end
for icp = 2:length(cp)
  cptotal = cptotal + (cp(icp)+cp(icp-1))*(t(icp)-t(icp-1))/2.0;
  if cp(icp) ~= 0
    yy(icp) = am(icp)/cp(icp);
    xx(icp) = cptotal/cp(icp);
  end
end
```

```
%%%%%%%%%%%%%%%%%%%%%%%%%%%%%%%%%%%%%%%%%%%%%%%%
%
% logan.m -- produce a logan plot for given pet and blood data
%
%  requires:
%     pet[n,2] -- column of times and column of measured pet data
%     blood[n,2] -- column of times and column of measured blood data
%
%  produces:
%     slope -- slope of Logan plot
%     intercept -- ordinate intercept of Logan plot
%
%%%%%%%%%%%%%%%%%%%%%%%%%%%%%%%%%%%%%%%%%%%%%%%%
%  evaluate Am, Cp and times from pet and blood data %
prepat
%  evaluate [x,y] points from Am, Cp and times  %
[xx,yy] = logan_pts(Am,Cp,AmCptimes);
%  setup initial [x,y] points through which to fit straight line %
xshort = xx; yshort = yy;
deltak = 1.0;
kold = 10;
ktolerance = 0.001;
%  loop until the difference in slope is less than ktolerance %
for ishort= 2:length(xx)
  k = polyfit(xshort,yshort,1);
  deltak = abs(k(1) - kold)/abs(k(1));
  if deltak < ktolerance, break, end
  kold = k(1);
  xshort = xx(ishort:length(xx));
  yshort = yy(ishort:length(yy));
end
point_1 = length(xx) - length(xshort)
slope = k(1)
intercept = k(2)
fit = polyval(k,xx);
plot(xx,yy,'o',xx,fit)
qltitle
```

```
%%%%%%%%%%%%%%%%%%%%%%%%%%%%%%%%%%%%%%%%%%%%%%%%
%
%  logan_pts.m -- calculate [x,y] pts for logan graphical analysis
%                 given Am, Cp and times
%
%%%%%%%%%%%%%%%%%%%%%%%%%%%%%%%%%%%%%%%%%%%%%%%%
function [xx,yy] = logan_pts(am,cp,amtimes)
cptotal = 0.0;
amtotal = 0.0;
clear xx yy;
% xx(1) = cp(1)/am(1);
% yy(1) = am(1)/am(1);
for iam = 2:length(am)
  cptotal = cptotal + ...
        (cp(iam)+cp(iam-1))*(amtimes(iam)-amtimes(iam-1))/2.0;
  amtotal = amtotal + ...
        (am(iam)+am(iam-1))*(amtimes(iam)-amtimes(iam-1))/2.0;
  yy(iam-1) = amtotal/am(iam);
  xx(iam-1) = cptotal/am(iam);
end
```

```
%%%%%%%%%%%%%%%%%%%%%%%%%%%%%%%%%%%%%%%%%%%%%%%%
%
%  sens.m -- calculate the mean and standard deviation for each of the
%            compartmental and graphical parameters
%
%  requires:
%     all the requirements of solve, patlak and logan
%     noise -- fractional expression of percent noise to add, e.g. 0.05
%     number -- number of iterations to run, e.g. 50
%
%  produces:
%     average[p] -- average parameters (k's)
%     deviation[p] -- standard deviation of each parameter
%     kcbar[2] -- average patlak slope and intercept, computed from k's
%     kcdev[2] -- standard deviation of above
%     kgbar[2] -- average patlak slope and intercept, graphical
%     kgdev[2] -- standard deviation of above
%
%%%%%%%%%%%%%%%%%%%%%%%%%%%%%%%%%%%%%%%%%%%%%%%%
global step_size
global model
global NCOMP
global pet
global coef
global times
global blood_lin
global brain_est
global cparam
global k_one
clear mins kcs pdiffs chis kgs;
count = 1;
%  set the random number generator to a normal distribution %
rand('normal')
%
%  set alpha such that, on average, the sqrt of the total counts
%  (the counts x the time interval), times alpha, gives "noise" percent
%
for i = 2:length(pet)
  time(i) = pet(i,1) - pet(i-1,1);
end
time(1) = time(2);
time = time*60;
alpha = noise*sqrt(mean(brain_est)*mean(time));
brainsave = brain_est;
petsave = pet;
%  add random noise to each point in pet data %
for inum = 1:number
  inum
  for j = 1:length(brain_est)
    pet(j,2) = brainsave(j) + ...
            rand(1)*alpha*sqrt(brainsave(j)/time(j));
  end
%  usually perform one of patlak or logan analysis %
  patlak;
% logan;
% disregard results of graphical analyses if point_1 is too far along %
  if point_1 <= length(Am)/2
    kgs(count,:) = k;
```

```
    count = count + 1;
  end
% save all the results %
  kmin = fmins('cost',param,tolerance,0);
  mins(inum,:) = kmin;
  [kcs(inum,1), kcs(inum,2)] = make_ki(kmin);
% [kcs(inum,1), kcs(inum,2)] = make_logan(kmin);
  pdiffs(inum) = pdiff(pet(:,1),pet(:,2),brainsave);
  chis(inum) = chisquare(brain_est,brainsave);
end
pet = petsave;
brain_est = brainsave;
% calculate and print means and standard deviations %
average = mean(mins)
deviation = std(mins)
kcbar = mean(kcs)
kcdev = std(kcs)
kgbar = mean(kgs)
kgdev = std(kgs)
mean_pdiff = mean(pdiffs)
mean_chi2 = mean(chis)
```

```
%%%%%%%%%%%%%%%%%%%%%%%%%%%%%%%%%%%%%%%%%%%%%%%%
%
%  covariance.m -- determine the standard deviations of the parameters
%                  using the covariance and the sensitivity matrix
%
%  requires:  that solve or once be run once before this routine is called
%
%  produces:  deltap[p] -- the estimated standard deviation of each param
%
%%%%%%%%%%%%%%%%%%%%%%%%%%%%%%%%%%%%%%%%%%%%%%%%
%  clear and reset initial values and useful constants %
clear rlparams S W deltap;
peps = .01;
dp = cost(min);
petend = length(pet);
%  create the (diagonal) weighting matrix %
W(1,1) = pet(2,1) - pet(1,1);
for iw = 2:petend-1
   W(iw,iw) = pet(iw+1,1) - pet(iw-1,1);
end
W(petend,petend) = pet(petend,1) - pet(petend - 1,1);
%  only evaluate for parameters that are non-zero %
rlparams = find(param~=0.0);
nparam = length(rlparams);
save_param = param;
save_est = brain_est;
%  compute the difference in the fitted curve at each point,
%   for an epsilon change in the parameter %
for iparam = 1:nparam
   param = save_param;
   param(rlparams(iparam)) = param(rlparams(iparam))*(1 + peps);
   brain_est = brainint(param);
   S(:,iparam)    =    (brain_est    -    save_est)/(param(iparam)    -
save_param(iparam));
end
param = save_param;
brain_est = save_est;
% compute the information matrix  %
M = S'*W*S;
ssq = dp/(petend - nparam);
%  compute the estimated standard deviations of the parameters  %
for iparam = 1:nparam
   deltap(iparam) = sqrt(ssq/M(iparam,iparam));
end
```

References

Agid, Y., (1991), "Parkinson's Disease: pathophysiology". *Lancet*, **337**: 1321-1324.

Agid, Y., Javoy, F., and Glowinski, J., (1973), "Hyperactivity of remaining dopaminergic neurones after partial destruction of the nigro-striatal dopaminergic system in the rat". *Nat. New. Bio.*, **245**: 150-151.

Axelrod, J., (1974), "Neurotransmitters". *Sci. Am.*, June 1974, 59-71.

Barrio, J. R., Huang, S.-C., Melega, W. P., et al., (1990), "6-[^{18}F]fluoro-L-DOPA probes dopamine turnover rates in central dopaminergic structures". *J. Neurosci. Res.*, **27**: 487-493.

Bertler, A., Falck, B., Owman, C., et al., (1966), "The localization of monoaminergic blood-brain barrier mechanisms". *Pharmocol. Rev.*, **18**: 369-385.

Bhatt, M. H., Snow, B. J., Martin, W. R. W., et al., (1991), "Positron emission tomography suggests that the rate of idiopathic parkinsonism is slow". *Ann. Neurol.*, **29**: 673-677.

Bradbury, M., (1979), *The Concept of a Blood-Brain Barrier*, Chichester: Wiley & Sons.

Brooks, D. J., Salmon, E. P., Mathias, C.J., et al., (1990), "The relationship between locomotor disability, autonomic dysfunction and the integrity of the striatal dopaminergic system in patients with multiple system atrophy, pure autonomic failure, and Parkinson's disease, studied with PET". *Brain*, **113**: 1539-1552.

Burnham, W. M., (1989), "Drugs acting on the basal ganglia". in Kalant, H. and Roschlau, W. H. E., (eds.), *Principles of Medical Pharmacology*, Toronto: Decker, 198-202.

Carson, E. R., Cobelli, C., and Finkelstein, L., (1983), *The Mathematical Modelling of Metabolic and Endocrine Systems*, New York: Wiley & Sons, 1-2.

Chan, G. L.-Y., Morrison, K. S., Holden, J. E., et al., (1992), "Plasma L-[^{18}F]6-fluorodopa input function: A simplified method". *J. Cereb. Blood Flow Metab.*, **12**: 881-884.

Chiueh, C. C., Burns, R. S., Kopin, I. J., et al., (1986), "6-^{18}F-DOPA/Positron Emission Tomography visualized degree of damage to brain dopamine in basal ganglia of monkeys with MPTP-induced Parkinsonism". in Markey, S.P., Castagnoli, N., and Kopin, I. J., (eds), *MPTP: A Neurotoxin producing a Parkinsonian Syndrome*, New York: Academic Press, 327-338.

Cho, Z. H., Chan, J. K., Ericksson, L., et al., (1975), "Positron ranges obtained from biomedically important positron-emitting radionuclides". *J. Nucl. Med.*, **16**: 1174-1176.

Cotzias, G. C., Van Woert, M. H., and Schiffer, L. M., (1967), "Aromatic Amino Acids and Modification of Parkinsonism". *New Eng. J. Med.*, **276**: 374-379.

Diffley, D. M., Costa, J. L., Sokoloski, E. A., et al., (1983), "Direct observation of 6-fluorodopamine in guinea pig nerve microsacs by ^{19}F NMR". *Biochem. Biophys. Res. Comm.*, **110**: 740-745.

DiStephano, J. J. III and Landaw, E. M., (1984), "Multiexponential, multicompartmental, and noncompartmental modeling. I. Methodological limitations and physiological interpretations". *Am. J. Physiol.*, **246**: R651-R664.

Doudet, D. J., McLellan, C. A., Aigner, T. G., et al., (1992), "Delayed L-phenylalanine infusion allows for simultaneous kinetic analysis and improved evaluation of specific-to-nonspecific fluorine-18-DOPA uptake in brain". *J. Nucl. Med.*, **33**: 1383-1389.

Doudet, D. J., McLellan, C. A., Carson, R., et al., (1991), "Distribution and kinetics of 3-O-Methyl-6-[^{18}F]fluoro-L-DOPA in the rhesus monkey brain". *J. Cereb. Blood Flow Metab.*, **11**: 726-734.

Eidelberg, D., (1992), "Positron Emission Tomography Studies in Parkinsonism". *Neurol. Clin.*, **10**: 421-433.

Enge, H. A., (1966), *Introduction to Nuclear Physics*, Reading, MA: Addison-Wesley, 232-235.

Evans, R. D., (1955), *The Atomic Nucleus*, New York: McGraw-Hill, 629-630.

Firnau, G., Sood, S., Chirakal, R., et al., (1987), "Cerebral metabolism of 6-[^{18}F]fluoro-L-3,4-dihydroxyphenylalanine in the primate". *J. Neurochem.*, **48**: 1077-1082.

Garnett, E. S., Firnau, G., Nahmias, C., et al., (1980), "Blood-brain barrier transport and cerebral utilization of dopa in living monkeys". *Am. J. Physiol.*, **238**: R318-R327.

Gjedde, A., Kuwabara, H., Reith, J., et al., (1992), "PET assay of dopa decarboxylase activity in living human brain". in the proceedings of *The Joint Meeting of the 4th International Trace Amines Conference and the 5th International Amine Oxidase Workshop*, Galway, Ireland, August 1992

Gjedde, A., Reith, J., Dyve, S., et al., (1991), "Dopa decarboxylase activity of the living human brain". *Proc. Natl. Acad. Sci.*, **88**: 2721-2725.

Gjedde, A., and Wong, D. F., (1990), "Modeling neuroreceptor binding of radioligands *in vivo*". in Frost, J. J. and Wagner, H. N. Jr., (eds.), *Quantitative Imaging: Neuroreceptors, Neurotransmitters, and Enzymes*, New York: Raven Press, 51-79.

Glowinski, J., (1976), "The use of L-3,5-[^{3}H]-tyrosine and the measurement of tritiated water to estimate DA turnover in central dopaminergic terminals". *Neuropharmacology*, **15**: 585-590.

Hartvig, P., Ågren, H., Reibring, L., et al., (1991), "Brain kinetics of L-[β-^{11}C]DOPA in humans studied by positron emission tomography". *J. Neural Transm.*, **86**: 25-41.

Hayden, T. L., Bourne, D. W. A., and Fu, Y. T., (1983), "Fourier-transform analysis of radiopharmaceutical data". *Math. Biosci.*, **63**: 71-85.

Hefti, F., Melamed, E., and Wurtman, R. J., (1981), "The site of dopamine formation in rat striatum after L-Dopa administration". *J. Pharmac. Exp. Ther.*, **217**: 189-197.

Herman, G. T., (1980), *Image Reconstruction from Projections*, New York: Academic Press.

Hjelle, J. T., Baird-Lambert, J., Cardinale, G., et al., (1978), "Isolated microvessels: The blood-brain barrier *in vitro*". *Proc. Nat. Acad. Sci.*, **75**: 4544-4548.

Hoffman, J. M., Melega, W. P., Hawk, T. C., et al., (1992), "The effects of carbidopa administration on 6-[^{18}F]fluoro-L-DOPA kinetics in positron emission tomography". *J. Nucl. Med.*, **33**: 1472-1477.

Horne, M. K., Cheng, C. H., and Wooten, G. F., (1984), "The cerebral metabolism of L-dihydroxyphenylalanine: An autoradiographic and biochemical study". *Pharmacology*, **28**: 12-26.

Hornykiewicz, O., (1963), "Die topische Lokalisation und das Verhalten von Noradrenalin und Dopamin (3-Hydroxytyramin) in der substantia nigra des normalen und Parkinsonkranken Menschen". *Wien. klin. Wchnschr.*, **75**: 309-312.

Huang, S.-C., Yu, D.-C., Barrio, J. R., et al., (1991), "Kinetics and modeling of L-6-[^{18}F]fluoro-DOPA in human positron emission tomographic studies". *J. Cereb. Blood Flow Metab.*, **11**: 898-913.

Itoh, M., Hatazawa, J., Ishiwata, K., et al., (1988), "Error Analysis in 6-^{18}F-DOPA brain influx rate measured by positron emission tomography". *CYRIC Ann. Rep.*, Cyclotron and Radioisotope Centre, Tohoku University, Japan, 261-265.

Itoh, M., Hatazawa, J., Ishiwata, K., et al., (1990), "Assessment of the ^{18}F-6-fluoro-L-DOPA influx rate to the brain in normal human subjects using positron emission tomography". *CYRIC Ann. Rep.*, Cyclotron and Radioisotope Centre, Tohoku University, Japan, 200-206.

Iversen, L. L., (1982), "Neurotransmitters and CNS Disease". *Lancet*, **2**: 914-918.

Javoy, F., Agid, Y., Bouvet, D., et al., (1974), "*In vivo* estimation of tyrosine hydroxylation in the dopaminergic terminals of the rat neostriatum". *J. Pharm. Pharmac.*, **26**: 179-185.

Knudsen, G. M., Pettigrew, K. D., Patlak, C. S., et al., (1990), "Asymmetrical transport of amino acids across the blood-brain barrier in humans". *J. Cereb. Blood Flow Metab.*, **10**: 698-706.

Korf, J., Grasduk, L., and Westernink, B. H. C., (1976), "Effects of electrical stimulation of the nigrostriatal pathway of the rat on dopamine metabolism". *J. Neurochem.*, **26**: 579-584.

Landaw, E. M., and DiStephano, J. J. III, (1984), "Multiexponential, multicompartmental, and noncompartmental modeling. II. Data analysis and statistical considerations". *Am. J. Physiol.*, **246**: R665-R677.

Lieberman, A., Estey, E., Gopinathan, G., et al., (1978), "Comparative effectiveness fo two extracerebral DOPA decarboxylase inhibitors in Parkinson disease". *Neurol.*, **28**: 964-968.

Lindvall, O., Brundin, P., Widner, H., et al., (1990), "Grafts of fetal dopamine neurons survive and improve motor function in Parkinson's disease". *Science*, **247**: 574-577.

Lloyd, K., and Hornykiewicz, O., (1970), "Parkinson's Disease: activity of L-dopa decarboxylase in discete brain regions". *Science*, **170**: 1212-1213.

Logan, J., Fowler, J. S., Volkow, N. D., et al., (1990), "Graphical analysis of reversible radioligand binding from time-activity measurements applied to [N-^{11}C-methyl]-(-)-Cocaine PET studies in human subjects". *J. Cereb. Blood Flow Metab.*, **10**:740-747.

Lovenberg, W., Weissbach, H., and Underfriend, S., (1962), "Aromatic L-amino acid decarboxylase". *J. Bio. Chem.*, **237**: 89-93.

Martin, W. R. W., Palmer, M. R., Patlak, C. S., et al., (1989), "Nigrostriatal function in humans studied with positron emission tomography". *Ann. Neurol.*, **26**: 535-542.

The MathWorks, Inc., (1990), *PRO-MATLAB User's Guide*, Natick, MA: The MathWorks, Inc.

McGeer, P. L. and Zeldowicz, L.R., (1990), "Administration of dihydroxyphenylalanine to Parkinsonian patients". *Canad. M. A. J.*, **90**: 463-466.

Melega, W. P., Grafton, S. T., Huang, S.-C., et al., (1991), "L-6-[^{18}F]fluoro-DOPA metabolism in monkeys and humans: Biochemical parameters for the formulation of tracer kinetic models with positron emission tomography". *J. Cereb. Blood Flow Metab.*, **11**: 890-897.

Melega, W. P., Hoffman, J. M., Luxen, A., et al., (1990), "The effects of carbidopa on the metabolism of 6-[^{18}F]fluoro-L-DOPA in rats, monkeys, and humans". *Life Sci.*, **47**: 149-157.

Melega, W. P., Hoffman, J. M., Schneider, J. S., et al., (1991), "6-[^{18}F]fluoro-L-DOPA metabolism in MPTP-treated monkeys: assessment of tracer methodologies for positron emission tomography". *Brain Res.*, **543**: 271-276.

Melega, W. P., Luxen, A., Perlmutter, M. M., et al., (1990), "Comparative *in vivo* metabolism of 6-[^{18}F]fluoro-L-DOPA and [^{3}H]L-DOPA in rats". *Biochem. Pharmacol.*, **39**: 1853-1860.

Nagatsu, T., Levitt, M., and Underfriend, S., (1964), "Tyrosine hydroxylase: The initial step in norepinephrine biosynthesis". *J. Bio. Chem.*, **239**: 2910-2917.

Nagatsu, T., Oka, K., Yamamoto, T., et al., (1981), "Catecholaminergic Enzymes in Parkinson's disease and related extrapyramidal diseases". in Riederer, P., and Usdin, E., (eds.), *Transmitter Biochemistry of Human Brain Tissue*, London: Macmillan, 291-302.

Nahmias, C., (1985), *A Clinical System for the measurement of Regional Metabolic Rates in the Brain*, Ph. D. thesis, University of Surrey.

Neff, N. H., and Hadjiconstantinou, M., (1992), "Modulation of aromatic L-amino acid decarboxylase activity". in the proceedings of *The Joint Meeting of the 4th International Trace Amines Conference and the 5th International Amine Oxidase Workshop*, Galway, Ireland, August 1992.

Papavasiliou, P. S., Cotzias, G. C., Düby, S., E., et al., (1972), "Levodopa in parkinsonism: Potentiation of central effects with a peripheral inhibitor". *New Eng. J. Med.*, **285**: 8-14.

Pate, B. D., Hewitt, K. A., Martin, W. R. W., et al., (1990), "*In vivo* studies of presynaptic dopaminergic function in non-human primates by PET-FD scanning". *Neurol.*, **40**: p. 264.

Pate, B. D., Snow, B. J., Hewitt, K. A., et al., (1991), "The Reproducibility of striatal uptake data obtained with positron emission tomography and fluorine-18-L-6-fluorodopa tracer in non-human primates". *J. Nucl. Med.*, **32**: 1246-1251.

Patlak, C. S., Blasberg, R. G., and Fenstermacher, J. D., (1983), "Graphical evaluation of blood-to-brain transfer constants from multiple-time uptake data". *J. Cereb. Blood Flow Metab.*, **3**: 1-7.

Patlak, C. S. and Blasberg, R. G., (1985), "Graphical evaluation of blood-to-brain transfer constants from multiple-time uptake data. Generalizations". *J. Cereb. Blood Flow Metab.*, **5**: 584-590.

Press, W. H., Flannery, B. P., Teukolsky, S. A., et al., (1986), *Numerical Recipes: The Art of Scientific Computing*, Cambridge: Cambridge University Press.

Provencher, S. W., (1976), "A Fourier method for the analysis of exponential decay curves". *Biophys. J.*, **16**: 27-41.

Reith, J., Dyve, S., Kuwabara, H., et al., (1990), "Blood-brain transfer and metabolism of 6-[^{18}F]fluoro-L-DOPA in rat". *J. Cereb. Blood Flow Metab.*, **10**: 707-719.

Sawle, G. V., Colebatch, J. G., Shah, A., et al., (1990), "Striatal function in normal aging: Implications for Parkinson's disease". *Ann. Neurol.*, **28**: 799-804.

Seeman, P., (1989), "Neuroleptics (Antipsychotics)" in Kalant, H. and Roschlau, W. H. E., (eds.), *Principles of Medical Pharmacology*, Toronto: Decker, 267-280.

Tedroff, J., Aquilonius, S.-M., Hartvig, P., et al., (1992), "Cerebral uptake and utilization of therapeutic [β-^{11}C]-L-DOPA in Parkinson's disease measured by positron imission tomography. Relations to motor response". *Acta. Neurol. Scand.*, **85**: 95-102.

Wade, L., and Katzman, R., (1975), "Rat brain regional uptake and decarboxylation of L-DOPA following carotid injection". *Am. J. Physiol.*, **228**: 352-359.

Westfall, T. C., Besson, M.-J., Giorguieff, J.-F., et al., (1976), "The role of presynaptic receptors in teh release and synthesis of ^{3}H-dopamine by slices of rat striatum". *Naunyn-Schmiedeberg's Arch. Pharmacol.*, **292**, 279-287.

Zierler, K., (1981), "A critique of compartmental analysis". *Ann. Rev. Biophys. Bioeng.*, **10**: 531-562.

Zierler, K., (1965), "Equations for measuring blood flow by external monitoring of radioisotopes". *Circulation Res.*, **16**: 309-321.